

## ON THE DEARTH OF COMPACT, MASSIVE, RED SEQUENCE GALAXIES IN THE LOCAL UNIVERSE

EDWARD N TAYLOR<sup>1,2</sup>, MARIJN FRANX<sup>1</sup>, KARL GLAZEBROOK<sup>3</sup>, JARLE BRINCHMANN<sup>1</sup>, ARJEN VAN DER WEL<sup>4</sup>, AND PIETER G VAN DOKKUM<sup>5</sup>

<sup>1</sup> Sterrewacht Leiden, Leiden University, NL-2300 RA Leiden, Netherlands; ent@strw.leidenuniv.nl, <sup>2</sup> School of Physics, the University of Melbourne, Parkville, 3010, Australia, <sup>3</sup> Centre for Astrophysics & Supercomputing, Swinburne University of Technology, Hawthorn, 3122, Australia <sup>4</sup> Max Planck Institut für Astronomie, D-69117 Heidelberg, Germany, <sup>5</sup> Department of Astronomy, Yale University, New Haven, CT 06520-8101

*Draft version October 8, 2018*

### ABSTRACT

Using data from the Sloan Digital Sky Survey (SDSS; data release 7), we have conducted a search for local analogs to the extremely compact, massive, quiescent galaxies that have been identified at  $z \gtrsim 2$ . We show that incompleteness is a concern for such compact galaxies, particularly for *low* redshifts ( $z \lesssim 0.05$ ), as a result of the SDSS spectroscopic target selection algorithm. We have identified 63  $M_* > 10^{10.7} M_\odot$  ( $\approx 5 \times 10^{10} M_\odot$ ) red sequence galaxies at  $0.066 < z_{\text{spec}} < 0.12$  which are smaller than the median size–mass relation by a factor of 2 or more. Consistent with expectations from the virial theorem, the median offset from the mass–velocity dispersion relation for these galaxies is 0.12 dex. We do not, however, find any galaxies with sizes and masses comparable to those observed at  $z \sim 2.3$ , implying a decrease in the comoving number density of these galaxies (at fixed size and mass) by a factor of  $\gtrsim 5000$ . This result cannot be explained by incompleteness: in the  $0.066 < z < 0.12$  interval, we estimate that the SDSS spectroscopic sample should typically be  $\gtrsim 75\%$  complete for galaxies with the sizes and masses seen at high redshift, although for the very smallest galaxies it may be as low as  $\sim 20\%$ . In order to confirm that the absence of such compact massive galaxies in SDSS is not produced by spectroscopic selection effects, we have also looked for such galaxies in the basic SDSS photometric catalog, using photometric redshifts. While we do find signs of a bias against massive, compact galaxies, this analysis suggests that the SDSS spectroscopic sample is missing at most a few objects in the regime we consider. Accepting the high redshift results, it is clear that massive galaxies must undergo significant structural evolution over  $z \lesssim 2$  in order to match the population seen in the local universe. Our results suggest that a highly stochastic mechanism like major mergers cannot be the primary driver of this strong size evolution.

*Subject headings:* galaxies: evolution—galaxies: formation—galaxies: fundamental parameters

### 1. INTRODUCTION

In the simplest possible terms, the naïve expectation from hierarchical structure formation scenarios is that the most massive galaxies form last. This is in contrast to the observation that the bulk of cosmic star formation occurs in galaxies with progressively lower stellar masses at later times (e.g. Juneau et al. 2005; Zheng et al. 2007; Damen et al. 2008); the so-called downsizing of galaxy growth. These observations have been accommodated within the  $\Lambda$ CDM framework with the introduction of a quenching mechanism (e.g. Menci et al. 2005; Croton et al. 2006; Cattaneo et al. 2008), which operates to shut down star formation in the most massive galaxies; this mechanism is also required to correctly predict the absolute and relative numbers of red galaxies (Dekel & Birnboim 2006; Bell et al. 2007; Faber et al. 2007). With this inclusion, models thus predict that a significant fraction of the local massive galaxy population should have finished their star formation relatively early in the history of the universe, with later mergers working to build up the most massive galaxies.

There is thus a crucial distinction to be made between a galaxy’s mean stellar age, and the time since that galaxy has assumed its present form (see, e.g., De Lucia et al. 2006): the most massive galaxies are expected to be both the oldest *and* the youngest galaxies. They are the oldest in the sense that their progenitors are expected to form

first in the highest cosmic overdensities—however, these stars are only assembled into their  $z = 0$  configuration relatively recently.

This leaves (at least) two open questions relating to the quenching of star formation and the formation and evolution of massive galaxies: 1.) When does star formation stop in massive galaxies, and 2.) What happens to galaxies after they have stopped forming stars?

In connection with the first of these questions, deep spectroscopic surveys have identified massive galaxies with little or no ongoing star formation at  $1 \lesssim z \lesssim 2$  (e.g. Cimatti 2004; Glazebrook et al. 2004; McCarthy 2004a; Daddi et al. 2004). At the same time, color selection techniques like the ERO (McCarthy 2004b, and references therein), DRG (Franx et al. 2003), or BzK (Daddi et al. 2005) criteria have been used to identify massive, passive galaxies at high redshifts. While these techniques are deliberately biased towards certain kinds of galaxies and certain redshift intervals, advances in techniques for photometric redshift estimation and stellar population modeling have allowed the selection of mass-limited samples, and so the construction of representative samples of the high redshift massive galaxy population (e.g. van Dokkum et al. 2006).

By obtaining very deep rest-frame optical spectra of a photometric-redshift selected sample of massive galax-

ies at  $z \gtrsim 2$ , Kriek et al. (2008a) made a significant advance on previous spectroscopic and photometric studies. Of the 36  $z_{\text{spec}} > 2$ ,  $M_* > 10^{11} M_{\odot}$  galaxies in the Kriek et al. (2008a) sample, 16 were shown unambiguously to have evolved stellar populations and little or no ongoing star formation. These galaxies also seem to form a red sequence in  $(B - V)$  color, although at low significance ( $3.3\sigma$ ; Kriek et al. 2008b). In other words, these massive galaxies appear both to have assembled stellar populations similar to galaxies of comparable mass in the local universe, and to have had their star formation effectively quenched.

Using Keck laser guide-star assisted adaptive optics and Hubble Space Telescope imaging, van Dokkum et al. (2008, hereafter vD08) measured sizes for 9 of the 16 strongly quenched galaxies from the Kriek et al. (2008a) sample. They found (rest-frame optical) effective radii in the range 0.5–2.4 kpc; that is, smaller than typical galaxies of the same mass in the local universe by factors of 3–10. These galaxies have stellar mass densities, measured within the central 1 kpc, which are 2–3 times higher than typical local galaxies of the same mass (Bezanson et al. 2009). Cimatti et al. (2008) and Damjanov et al. (2009, hereafter D09) have found similarly compact sizes for massive galaxy samples drawn from  $1 < z < 2$  spectroscopic surveys. Further, van Dokkum, Kriek & Franx (2009) have recently measured a velocity dispersion of  $510^{+165}_{-95}$  km/s for one of the galaxies in the vD08 sample, based on a 29 hr NIR spectrum; this extremely high value is consistent with the galaxy’s measured mass and size. (See also Cappellari et al. 2009.)

By providing rest-frame optical size measurements for a representative, mass-limited sample of galaxies spectroscopically-confirmed to have little or no ongoing star formation and  $z \gtrsim 2$ , these results confirm and consolidate the work of Daddi et al. (2005), Trujillo et al. (2006), Trujillo et al. (2007), Zirm et al. (2007), and Toft et al. (2007), as well as  $1 < z < 2$  results from, e.g., Longhetti et al. (2007) and Saracco et al. (2009), and  $z \lesssim 1$  results from van der Wel et al. (2008). (See also Buitrago et al., 2008.)

The significance of these results is that while the massive and largely quiescent galaxies at  $z \gtrsim 2$  have stellar populations that are consistent with their being more or less ‘fully formed’ early type galaxies, they must *each* undergo significant structural evolution in order to develop into galaxies like the ones seen in the local universe. Taken together, these results thus paint a consistent picture of strong size evolution among massive, early type and/or red sequence galaxies<sup>1</sup>—both as a population and individually—even after their star formation has been quenched (see also Franx et al. 2008). Whatever the mechanism for this growth in size (see, e.g., Fan et al. 2008; Hopkins et al. 2009; Naab et al. 2009; Khochfar & Silk 2009), the formation of massive, passive galaxies is not monolithic.

The aim of this paper is to test the proposition that

<sup>1</sup> There is considerable, but not total, overlap between color-selected samples of red sequence galaxies, and morphology-selected samples of early type galaxies. While it is common to use these terms as if they were more or less interchangeable, it should be remembered that they are not.

there are no galaxies in the local universe with sizes and masses comparable to those found at  $z \gtrsim 1.5$  — this is the crux of the argument against the monolithic formation of massive galaxies. This work is based on the latest data products from the Sloan Digital Sky Survey (SDSS; York et al. 2000; Strauss et al. 2002). In particular, we will focus on the possibility that such galaxies have been overlooked in SDSS due to selection effects associated with the construction of the spectroscopic target sample.

The structure of this paper is as follows: We describe the basic SDSS data that we have used in §2. In §3, we define our sample of compact galaxy candidates, and present several checks to confirm that these galaxies are indeed unusually small for their stellar masses. Then, in §4, we consider the importance of the SDSS spectroscopic selection for massive, compact galaxies. In this Section, we also compare our  $z \sim 0.1$  compact galaxy candidates with the vD08 and D09 samples. In Appendix A, we provide a complementary analysis in order to confirm our conclusion that the apparent differences between the high- and low-redshift samples cannot be explained by selection effects, including an estimate for the number of compact galaxies that may be missing from the SDSS spectroscopic sample. Finally, in §5, we compare our results to a similar studies by Trujillo et al. (2009) and Valentinuzzi et al. (2009), and briefly examine the properties of our compact galaxies’ stellar populations in comparison to the general  $z \sim 0.1$  red sequence galaxy population. A summary of our main results is given in §6. Throughout this work, we assume the concordance cosmology; *viz.*:  $\Omega_m = 0.3$ ,  $\Omega_{\Lambda} = 0.7$ , and  $H_0 = 70$  km/s/Mpc.

## 2. BASIC DATA AND ANALYSIS

The present work is based on Data Release 7 (DR7; Abazajian et al. 2009) of the SDSS, accessed via the Catalog Archive Server<sup>2</sup> (CAS; Thakar et al. 2008). In this section, we describe the basic SDSS data that we have used, and our analysis of it. We will search for compact galaxy candidates in the SDSS spectroscopic catalog; to this end, we will only consider `sciencePrimary` objects (a flag indicating a ‘science-grade spectrum, and weeding out multiple observations of individual objects) with either a ‘star’ or ‘galaxy’ photometric type (*i.e.*, a genuine astronomical source). The details of the SDSS spectroscopic sample selection are given in Strauss et al. (2002); we will summarize the most relevant aspects of this process in §4.1.

### 2.1. The Basic SDSS Catalog

For the basic SDSS catalog, there are two different methods for performing photometry. The first, the ‘Petrosian’ magnitude, is derived from the observed, azimuthally averaged (1D) light profile. The Petrosian radius is defined as the point where the mean surface brightness in an annulus drops to a set fraction (*viz.* 0.2) of the mean surface brightness within a circular aperture of the same radius. Within SDSS, the Petrosian aperture is defined to be twice the Petrosian radius; this aperture will contain 99 % of the total light for a well resolved exponential disk, but may miss as much as 18 % of

<sup>2</sup> <http://casjobs.sdss.org/CasJobs/>

the light for a de Vaucouleurs  $R^{1/4}$  profile (Strauss et al. 2002; Blanton et al. 2005).

The second photometric measure is derived from fits to the observed (2D) distribution of light in each band, using a sector-fitting technique, in which concentric annuli are divided into 12  $30^\circ$  sectors, as described in Appendix A.1 of Strauss et al. (2002). These fits are done assuming either an exponential or a de Vaucouleurs profile, convolved with a fit to the appropriate PSF. For each profile, the structural parameters (*viz.* axis ratio, position angle, and scalelength) are determined from the  $r$  band image. The more likely (in a  $\chi^2$  sense) of the two profile fits is used to define ‘model’ magnitudes for each galaxy. For the *ugriz* bands, these parameters are then held fixed, and only overall normalization (*ie.* total flux) is fit for.

The basic catalog also provides two different measures of size, associated with these two magnitude measurements. The Petrosian half-light radius,  $R_{50}$ , is defined as the radius enclosing half the ‘total’ Petrosian flux. The catalog also contains best fit structural parameters, including the effective radius, from a separate set of fits to each band independently, again for both an exponential and a de Vaucouleurs profile. Note that whereas the Petrosian magnitude and size are derived from the observed, PSF-convolved radial profile, the model values provide a PSF-corrected measure of the intrinsic size.

We use model magnitudes to construct *ugriz* SEDs for each object, since these measurements are seeing-corrected. From DR7, the basic SDSS photometric calibration has been refined so that the photometry is given in the AB magnitude system without the need for any further corrections (Padmanabhan et al. 2008). For measuring sizes, we will rely on the best-fit model effective radius,  $R_e$ , as determined from the  $z$  band. We also adopt a minimum measured size of  $0''.75$ , corresponding to half the median PSF FWHM for the SDSS imaging; we will plot all galaxies with observed sizes smaller than  $0''.75$  as upper limits. (None of our conclusions depend on the choice of this limit, which ultimately affects only 5 of our lower-mass compact galaxy candidates.)

## 2.2. Derived Quantities

We have derived rest-frame photometry for each object, based on its observed *ugriz* SED and redshift, using the IDL utility InterRest (Taylor et al. 2009), with a redshift grid of  $\Delta z = 0.001$ . In order to minimize the  $k$ -corrections and their associated errors, we determine rest-frame photometry through the *ugriz* filters redshifted to  $z = 0.1$ , which we denote with a superscript 0.1. We estimate that the systematic uncertainties are at the level of  $\lesssim 0.02$  mag. The agreement between our interpolated rest-frame photometry and that derived using the SDSS *kcorrect* algorithm (Blanton & Roweis 2007) is very good: our derived ( $u - r$ ) colors are  $\sim 0.02$  mag bluer for blue galaxies, and  $\sim 0.03$  mag redder for red galaxies.

We make use of stellar mass estimates provided by the MPA Garching group.<sup>3</sup> JB has fit the *ugriz* photometry of all galaxies using the synthetic stellar population library described by Gallazzi et al. (2005), based on Bruzual & Charlot (2003) models and assuming a

Chabrier (2003) stellar initial mass function (IMF) in the range  $0.1\text{--}100 M_\odot$ . The Gallazzi et al. (2005) library contains a large number of Monte Carlo realizations of star formation histories, parameterized by a formation time ( $1.5 < t_{\text{form}}/[\text{Gyr}] < 13.5$ ), an exponential decay rate ( $0 < \gamma/[\text{Gyr}^{-1}] < 1$ ), and including a number of random star formation bursts (randomly distributed between  $t_{\text{form}}$  and 0, normalized such that 10 % of galaxies experience a burst in the last 2 Gyr). In the fitting, the photometry has been corrected for emission lines under the assumption that the global emission line contribution is the same as in the spectroscopic fiber aperture.

The agreement between these SED-fit mass estimates and those of Kauffmann et al. (2003a), which were derived from spectral line indices, are excellent: the median offset is  $-0.01$  dex, with a scatter on the order of 0.1 dex. For the highest masses, however, the SED-fit results are slightly less robust: for  $M_* > 10^{11} M_\odot$ , the median formal error is  $\lesssim 0.10$  dex, compared to  $\lesssim 0.06$  dex for the Kauffmann et al. (2003a) estimates.

In the upper panel of Figure 1, we show the stellar mass to light ratios,  $M_*/L_i$ , for  $0.066 < z < 0.12$  galaxies as a function of their  $^{0.1}(g - i)$  color; here again,  $L_i$  should be understood as referring to the  $i$ -band filter redshifted to  $z = 0.1$ , or  $^{0.1}i$ . Notice that, at least for these mass estimates,  $M_*/L$  is a very tight function of color. In the main panel of this Figure, the red line shows the median  $M_*/L_i$  in narrow color bins. Making a simple linear fit to these points, we find:

$$\log(M_*/L_i) = -0.82 + 0.83 \times ^{0.1}(g - i), \quad (1)$$

where both  $M_*$  and  $L_i$  are in solar units. (The absolute

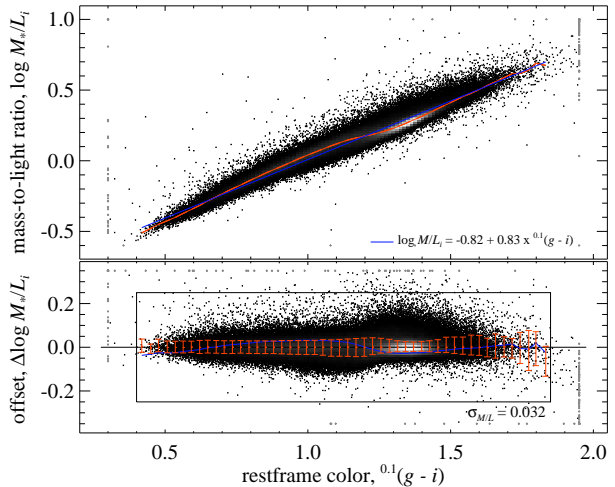


FIG. 1.— The mass-to-light ratios,  $M_*/L_i$ , of  $0.066 < z < 0.12$  galaxies as a function of their  $(g - i)$  color. (Here,  $M_*/L_i$  is understood to relate to the  $i$  band redshifted to  $z = 0.1$ .) The greyscale shows the (linear) data density in cells, where the data density is high. In the main panel, the red line shows the median  $M_*/L_i$  in narrow color bins; the blue line is a linear fit to these points. In the lower panel, we have simply subtracted away the median relation; in this panel, the error bars show the 16/84 percentiles in color bins. The simple linear relation shown provides an acceptable description of the observed relation, to within 0.02–0.04 dex; the global RMS offset from this relation is 0.032 dex. In order to avoid selecting ‘catastrophic failures’ in terms of stellar mass estimates, we will consider only those galaxies that fall within 0.25 dex of the median  $M_*/L_i$ – $^{0.1}(g - i)$  relation, and with  $0.4 < ^{0.1}(g - i) < 1.8$ , as shown by the box in the lower panel.

<sup>3</sup> Available via <http://www.mpa-garching.mpg.de/SDSS/DR7>.

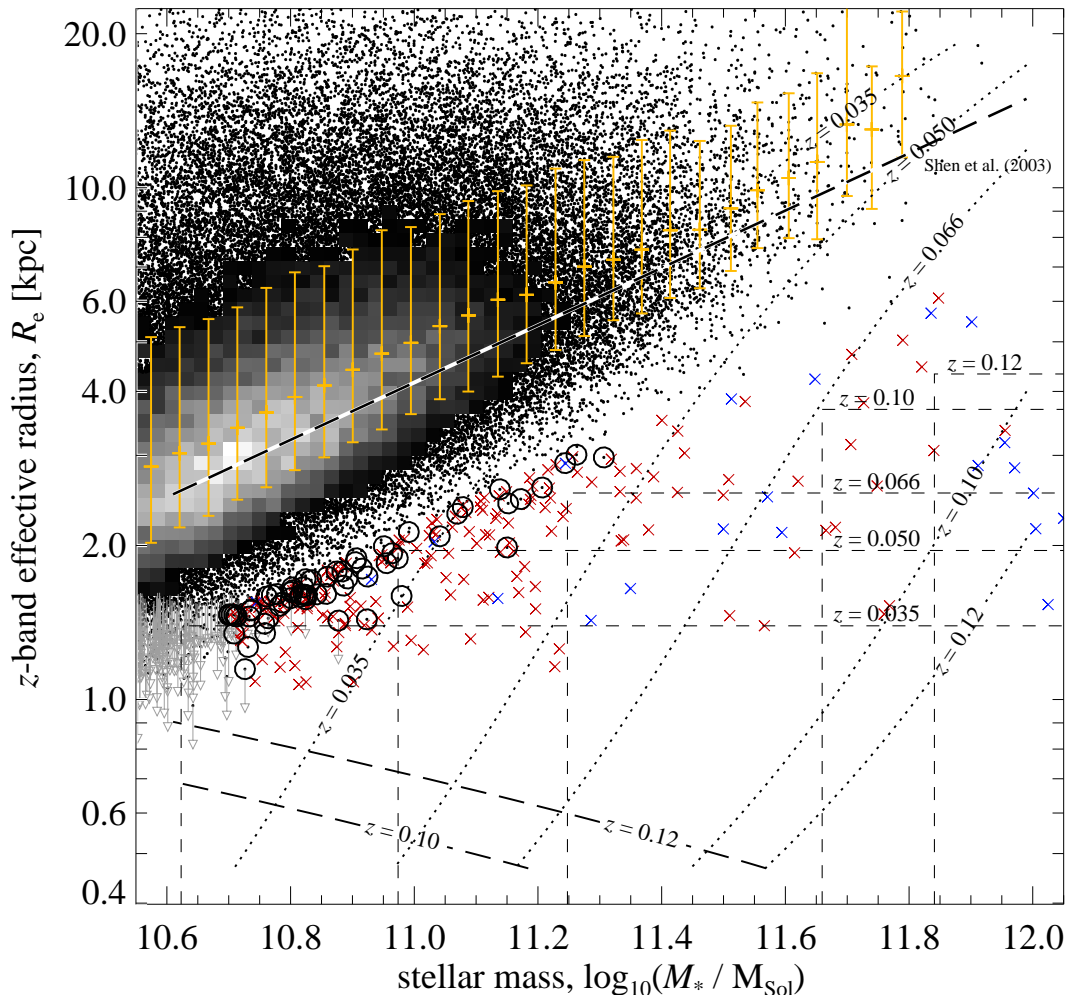


FIG. 2.— The size–mass relation for massive, red sequence galaxies showing the importance of the SDSS spectroscopic selection criteria. The points show SDSS galaxies ( $0.066 < z < 0.12$ ) selected to have  $^{0.1}(u-r) > 2.5$ . The yellow points show the median size in narrow bins of stellar mass; the error bars show the 16/84 percentiles in each bin. A fit to this median size–mass relation for red sequence galaxies is consistent with the Shen et al. (2003) relation for early type galaxies (dashed line), albeit offset by 0.05 dex. Individual galaxies that we have visually inspected ( $M_* > 10^{10.7} M_\odot$ ;  $\Delta \log R_e < -0.3$  dex) are marked with large symbols. Galaxies with  $M/L$ s that differ significantly from the main color– $M/L$  relation shown in Figure 1 are marked with small blue crosses. Galaxies with obvious problems in their photometry (especially those affected by the presence of a bright nearby star or blended with other galaxies) are marked with a small red cross; those that look okay are plotted as circles. Galaxies with observed sizes smaller than  $0''.75$  are plotted as upper limits, assuming a size of  $0''.75$ . The different lines show how the principal selection limits for spectroscopic followup translate onto the  $(M_*, R_e)$  plane for  $z = 0.12, 0.10, 0.066, 0.050$ , and  $0.35$  (top to bottom): the diagonal, long-dashed lines show the star/galaxy discriminator; the short-dashed boxes show the ‘saturation’ selection limit, and the diagonal dotted lines show the ‘cross-talk’ selection limit (see §4.1 for a detailed discussion). Galaxies lying below these lines will not be targeted spectroscopically.

magnitude of the sun in the  $^{0.1}i$  band is 4.58.) This relation is shown in Figure 1 as the solid blue line. We present this relation as an alternative to the popular Bell & de Jong (2001) or Bell et al. (2003) relations.

In the lower panel of Figure 1, we show the dispersion around the median relation; in this Figure, the error bars show the 16/84 percentiles in bins of color. Overall, the dispersion around this relation is just 0.032 dex. Note that while the simple linear relation given above provides an acceptable description of the ‘true’ relation, systematic offsets exist at the 0.02–0.04 dex level. The global mean and random offset from this linear relation are 0.002 dex and 0.040 dex, respectively.

In both panels, the small grey pluses show points that

fall outside the plotted range. Notice that there are a small fraction of galaxies that fall well off the main  $M_*/L$ –color relation, some by an order of magnitude or more. These galaxies also lie significantly off the main stellar mass–dynamical mass relation and are very likely to represent catastrophic failures of the stellar mass SED-fitting algorithm. This presents a problem when it comes to looking for outliers in the mass–size plot: selecting the most extreme objects may well include those objects with the largest errors. For this reason, we will restrict our attention to those objects that fall within 0.25 dex ( $\approx 7.8\sigma$ ) of the main  $M_*/L$ –color relation, and with  $0.2 < ^{0.1}(g-i) < 1.8$ , as shown by the box in the lower panel of Figure 1. This selection excludes just

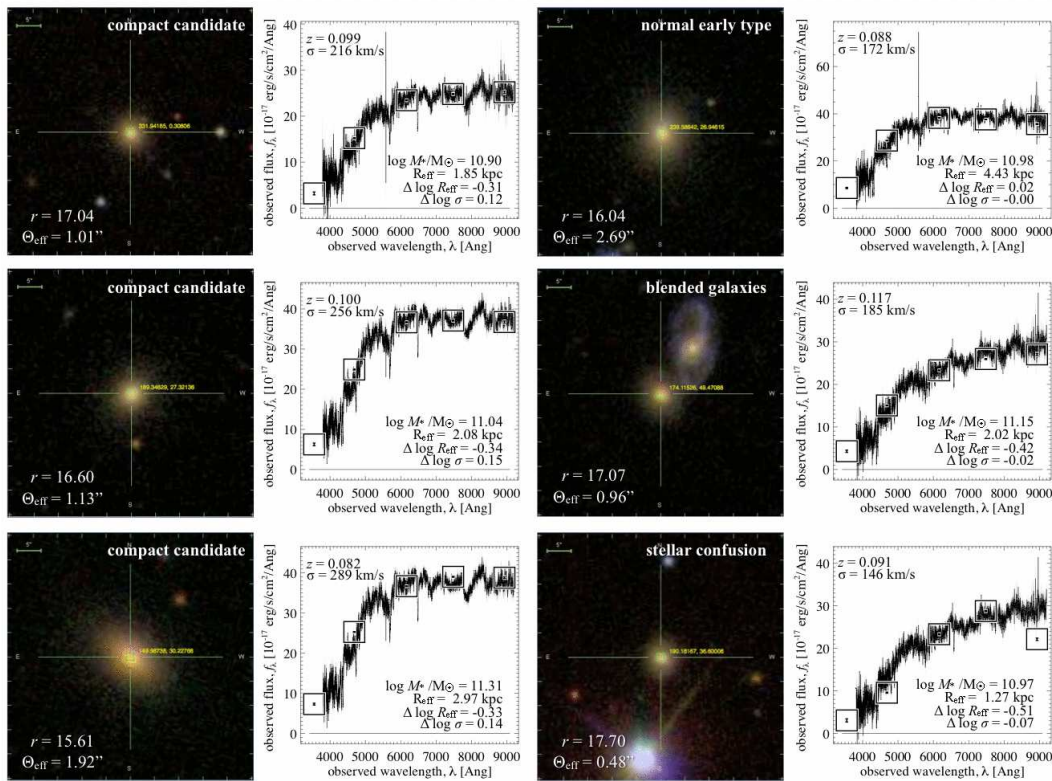


FIG. 3.— Illustrative examples of the galaxies we consider. Clockwise from the top-right, we show a ‘normal’, massive early type galaxy that lies very close to the median size–mass and velocity dispersion–mass relations, two compact galaxy candidates where visual inspection suggested problematic size measurements, and three of our compact galaxy candidates. Each of the three compact galaxy candidates shown in this Figure have observed velocity dispersions that are approximately consistent with their small measured sizes (see §3.3). For each galaxy, we show the SDSS SkyServer thumbnail image used for visual inspection, as well as the galaxies’ observed spectra; the boxes show the SEDs from the photometry, scaled to match the spectroscopic flux in the  $r$  band.

under 600 of the 223292 galaxies shown in Figure 1.

### 3. SEARCHING FOR MASSIVE, COMPACT, EARLY-TYPE GALAXIES IN THE LOCAL UNIVERSE

#### 3.1. Identifying Massive, Compact Galaxy Candidates

Figure 2 shows the size–mass plot for a sample of massive, red-sequence galaxies drawn from the SDSS DR7 spectroscopic sample. These galaxies have been selected to have  $^{0.1}(u-r) > 2.5$  and  $0.066 < z < 0.12$ . These redshift limits have been chosen to minimize the importance of selection effects and measurement biases, which we will discuss in §4.1. For now, we note that, mapping the  $r < 17.77$  spectroscopic limit onto  $M_*(z)$ , we should be highly complete (volume limited) for  $M_* > 10^{10.7} M_\odot$  and  $z < 0.12$ . As a very simple check on this, we note that for this sample, the median redshift in narrow bins of stellar mass is within the range  $z = 0.098$ – $0.102$  for all  $M_* > 10^{10.7} M_\odot$ ; the volumetric center of the  $0.066 < z < 0.12$  bin is  $z = 0.10$ .

The yellow points in this Figure show the median size in narrow bins of stellar mass; the error bars show the 14/86 percentiles. For comparison, the long-dashed line shows the local size–mass relation for early-type galaxies from Shen et al. (2003), corrected for differences in assumed IMF and cosmology. Contrary to the findings of Valentuzzi et al. (2009), a simple fit to the size–mass relation for *red sequence* galaxies ( $^{0.1}(u-r) > 2.5$ ) shown in Figure 2 is consistent with the Shen et al. (2003) re-

lation for *early type* ( $n > 2.5$ ) galaxies, albeit offset in size by 0.05 dex or, equivalently, by  $-0.09$  dex in mass. At fixed mass, the mode of the distribution is similarly offset (see Figure 7); this does not appear to be due to large numbers of late type galaxies in the sample.

We next select and study very compact galaxies from within the red sequence sample shown in Figure 2. At first glance, it appears that there may be a few galaxies that lie well below the main size–mass relation. However, it must be remembered that by selecting the most extreme outliers, we will also be selecting those objects with most egregious measurement errors.

For this reason, we have individually visually inspected all  $M_* > 10^{10.7} M_\odot$  galaxies with inferred sizes that are less than half the size predicted from the Shen et al. (2003) relation; *ie.*  $\Delta R_e < -0.3$  dex. For sizes smaller than the median relation, the distribution of sizes around the Shen et al. (2003) relation is very well described by a Gaussian with  $\sigma = 0.11$  dex; this  $\Delta R_e$  cut thus corresponds to selecting those galaxies whose sizes are smaller than the mean size (at fixed mass) at the  $\gtrsim 2.7\sigma$  level. (Adopting our own fit to the size–mass relation, this selection translates to  $\Delta R_e < -0.35$  dex; our results are otherwise unchanged.)

We have inspected 280 such objects, and discarded those where there are obvious reasons to distrust the size measurements. The most common reasons for discarding galaxies were confusion with other galaxies (99 galaxies, including 19 good merger candidates, and two possible

TABLE 1  
 PROPERTIES OF OUR COMPACT GALAXY CANDIDATES

RA (1) <sup>a</sup>	dec (2) <sup>a</sup>	$z$ (3) <sup>a</sup>	$(u-r)_{\text{obs}}$ (4) <sup>a</sup>	$^{0.1}(u-r)$ (5)	$\log M_*$ (6) <sup>b</sup>	$\Theta_{50,z}$ (7) <sup>a</sup>	$n$ (8) <sup>c</sup>	$\Theta_{50,z}$ (9) <sup>c</sup>	$R_e$ (10)	$\sigma$ (11) <sup>b</sup>	$T$ (12) <sup>d</sup>	$Z$ (13) <sup>d</sup>
190.16652	13.81563	0.0855	2.577	2.642	10.700	0.912	4.31	0.917	1.462	160	...	...
127.02722	55.37988	0.0665	2.828	2.999	10.701	1.152	3.26	1.211	1.468	191	...	...
225.31708	30.58266	0.0980	2.858	2.877	10.705	0.808	3.87	0.773	1.464	195	...	...
227.08531	7.25325	0.0764	2.963	3.113	10.709	0.929	5.13	1.188	1.345	199	...	...
215.41043	40.03233	0.0998	2.803	2.813	10.709	0.795	4.11	0.670	1.464	176	9.775	0.035
222.12988	26.48791	0.1058	2.549	2.540	10.712	0.750	4.65	0.722	1.453	155	...	...
118.81702	33.22864	0.0980	2.680	2.697	10.713	0.803	2.67	0.739	1.454	154	-99	-99
143.05707	11.70454	0.0811	2.690	2.776	10.726	0.750	5.52	0.830	1.146	166	9.255	0.132
204.66577	59.81854	0.0704	2.857	3.012	10.731	0.943	3.92	0.974	1.267	235	9.845	0.229
230.28553	24.21978	0.0809	2.922	3.028	10.733	0.952	5.90	1.298	1.453	153	...	...

NOTE. — We give only the first ten candidates here; the properties of the full sample of 63 galaxies is available as an electronic table via <http://www.strw.leidenuniv.nl/~ent/>. Col.s (1) and (2): position in decimal degrees (J2000); Col. (3) spectroscopic redshift; Col.s (4) and (5): observed and rest-frame colors; Col. (6) stellar mass in units of solar masses; Col. (7) apparent De Vaucouleurs effective radius in arcsec; Col. (8) and (9) Sérsic index and apparent Sérsic effective radius in arcsec; Col. (10) physical De Vaucouleurs effective radius in kpc; Col. (11) velocity dispersion in km/s; Col. (12) luminosity-weighted age in Gyr; Col. (13) mean metallicity. In Col.s (12) and (13), data is only given for those objects that appear in DR4; values of -99 indicate unsuccessful fits to the spectra. SOURCES. — <sup>a</sup>: the default SDSS (York et al. 2000; Strauss et al. 2002) catalog for DR7 (Abazajian et al. 2009), accessed via CAS (Thakar et al. 2008); <sup>b</sup>: the MPA-JHU catalog for DR7 (accessible via <http://www.mpa-garching.mpg.de/SDSS/DR7/>); <sup>c</sup>: the NYU VAGC (Blanton et al. 2005) for DR7; <sup>d</sup>: the stellar age and metallicity catalog of Gallazzi et al. (2005) for DR4.

lenses), or with the extended halos, diffraction spikes, and/or reflections of bright stars (62 galaxies). A further 19 galaxies were clearly disk-like, 5 showed marked asymmetries, and 1 had a very strong AGN spectrum; these candidates were also discarded. We discarded a further 3 objects with bad or missing data.

In Figure 3, we show several illustrative examples of the galaxies we are considering. On the right-hand side of this Figure, we show a ‘normal’ early type galaxy, with  $M_* \approx 10^{11} M_\odot$ , which falls very close to the Shen et al. (2003) relation. Below this, we show two of the compact galaxy candidates that we have rejected on the basis of visual inspection. On the left-hand side of this Figure, we show three of the compact galaxy candidates of different stellar masses that we have retained after visual inspection. For each galaxy, we show the thumbnail image from the SDSS SkyServer<sup>4</sup>, used for visual inspection. We also show each galaxy’s observed spectrum and photometry; here, we have scaled the photometry to match to the integrated  $r$ -band flux from the observed spectrum.

In addition to these galaxies with suspect size measurements, we have excluded a further 27 galaxies whose SED-fit  $M_*/L_s$  are offset from the main color- $M_*/L$  relation shown in Figure 1 by more than 0.25 dex. If we use Equation 1 to derive new stellar mass estimates for these galaxies, all of these galaxies move back into the main cloud in both Figure 2 and a stellar mass-dynamical mass plot, with mean/median offsets of  $\lesssim 0.02$  dex in both cases.

The 190 galaxies discarded on the basis of inspection are shown in Figure 2 as small red crosses; the small blue crosses show the 27 galaxies with discrepant  $M_*/L_s$ . As a function of  $\Delta R_e$ , the fraction of inspected sources that

have been discarded goes fairly smoothly from 60 % for  $\Delta R_e \sim -0.3$  dex to  $\sim 100$  % for  $\Delta R_e < -0.5$  dex. The discarded fraction has a similar dependence on mass: it is  $\sim 60$  % for  $M_* \sim 10^{10.7} M_\odot$ , rising to  $\sim 85$  % for  $M_* \sim 10^{11} M_\odot$ , and 100 % for  $M_* > 10^{11.4} M_\odot$ .

This leaves us with a sample of 63 massive, compact, early-type and red sequence galaxy candidates; these are marked in Figure 2 with heavy black circles. Of those galaxies that we have retained, 8 % (5/63) have observed sizes smaller than  $0''.75$ ; all of these have  $M_* < 10^{11} M_\odot$ . We have provided the properties of our compact galaxy candidates in Table 1.

### 3.2. Are the Size Measurements Wrong?

We have performed a number of checks to validate the small measured sizes of our compact galaxy candidates. The compact galaxy candidates do not have significantly larger size measurement errors in comparison to the full sample shown in Figure 2. For both the  $r$ - and  $z$ -bands, our candidates are not anomalous in a plot of Petrosian half-light radius versus model effective radius, nor are they anomalous in a plot of  $r$ -band size versus  $z$ -band size. For all but two of the candidates, the Petrosian and model magnitudes agree to within 0.15 mag. The mean offset between model and Petrosian magnitudes is -0.06 mag for the compact galaxies, compared to -0.08 mag for the full sample shown in Figure 2. That is, the compact candidates appear to be well described by the de Vaucouleurs model fits.

For the New York University (NYU) Value Added Galaxy Catalog (VAGC), Blanton et al. (2005) have fit the radially-averaged light profiles of each object, fitting for the Sérsic index as a free parameter over the range  $0 \leq n < 6$ . In order to explore further the issue of the quality of the de Vaucouleurs profile fits, we have gone

<sup>4</sup> Also accessible via CAS at <http://cas.sdss.org>.

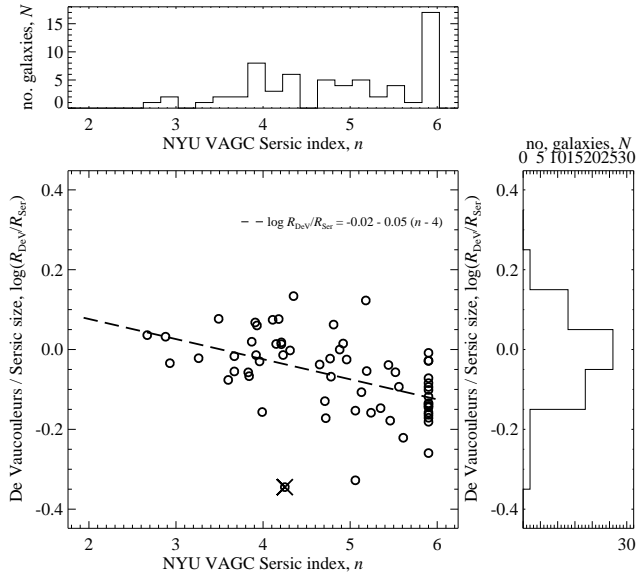


FIG. 4.— Comparison between effective radii derived assuming a de Vaucouleurs ( $n = 4$ ) profile and assuming a Sérsic profile ( $0 < n < 6$ ). Whereas the basic SDSS catalog uses a sector-fitting technique to fit either an exponential ( $n = 1$ ) or a de Vaucouleurs ( $n = 4$ ) profile, for the NYU VAGC, Blanton et al. (2005) have fit the radial profiles of each object assuming a general Sérsic model ( $0 < n < 6$ ). This Figure shows the ratio of these two sizes for our compact galaxy candidates, based on the  $z$ -band data, as a function of Sérsic index  $n$ . Almost all candidates have  $n > 3$ —these galaxies are not obviously exponentials. However, approximately 25 % have  $n = 5.9$ ; the maximum value allowed in the Blanton et al. (2005) fits. For these galaxies, the median ratio between the two size measurements is 0.88, with an RMS scatter of 0.1 dex. In the main panel, we show a least-squares fit to the data, the dispersion around this relation is  $\lesssim 0.1$  dex.

to the NYU VAGC for DR7, and looked up the Sérsic fit results for each of our candidates.

In Figure 4, we show the distribution of Sérsic parameters for our candidates, as well as a comparison between the Sérsic and de Vaucouleurs sizes. First, we note that nearly all (59/63) of our compact galaxy candidates have  $n > 3$ ; these are not late-type (exponential) galaxies. It is therefore unsurprising—but still reassuring—that the two size measures agree quite well: for the median galaxy among our candidates, the de Vaucouleurs size is  $\sim 10\%$  smaller than the Sérsic size; the RMS dispersion is 0.10 dex. For comparison, the median quoted error for the de Vaucouleurs size measurements is 4.6%.

Notice that about a quarter (17/63) of our candidates have  $n = 5.9$  in the NYU VAGC; this is the maximum value allowed in the fits. These galaxies are considerably more centrally-concentrated than the canonical de Vaucouleurs  $R^{1/4}$ -law profile. However, the trend with increasing Sérsic index is for the de Vaucouleurs size,  $R_{\text{DeV}}$ , to be systematically lower than the Sérsic size,  $R_{\text{Ser}}$ : making a least-squares fit to the data shown in Figure 4, we find  $\log R_{\text{DeV}}/R_{\text{Ser}} = -0.02 - 0.05(n - 4)$ . If these galaxies do have  $n > 6$ , then we may well be underestimating their sizes by  $\gtrsim 25\%$ .

Guo et al. (2009) have recently demonstrated that as a result of biases in the way the background sky level is estimated for the Sérsic fitting, the NYU-VAGC sizes are systematically underestimated at the  $\gtrsim 15\%$  level for  $n \gtrsim 5$ . This problem is progressively worse for large

sizes ( $\Theta_e \gtrsim 1''$ ) and bright magnitudes ( $r \lesssim 16$ ); for our compact galaxy candidates, the effect is likely to be at the  $\sim 20\%$  level. But note this implies that the difference between the de Vaucouleurs and Sérsic sizes is even greater than Figure 4 might suggest: the sizes of the  $n \gtrsim 5$  compact galaxies may be underestimated by as much as  $\gtrsim 30\%$ .

As a final check, therefore, we have also re-derived Sérsic effective radii for our compact galaxy candidates using GALFIT (Peng et al. 2002) and done a similar comparison as for the NYU VAGC sizes. The agreement between the GALFIT and VAGC Sérsic indices is quite good, with an rms difference in  $n$  of 1.1. Again the vast majority of objects have  $n > 3$ . There are 19 objects that are assigned the maximum allowed value of  $n = 8$ , but only 9 of these have  $n = 5.9$  in the VAGC. Making a similar fit to the difference between the default De Vaucouleurs and the GALFIT Sérsic effective radii, we find  $\log R_{\text{DeV}}/R_{\text{Ser}} = 0.08 - 0.08(n - 4)$ . As before, we may be underestimating the sizes of high  $n$  galaxies by 10–35 %, although this comparison suggests that we may also be overestimating the sizes of the few candidates with  $n < 4$ . The median galaxy has a GALFIT Sérsic effective radius 15 % smaller than the default De Vaucouleurs value. Lastly, we note that there is a definite mass-dependence to the agreement between the GALFIT Sérsic and default De Vaucouleurs effective radii, such that all but one of the galaxies for which the sizes agree to within 20 % have  $M_* > 10^{11} M_\odot$ .

To summarize the results of this section, then: comparison to 1D and 2D Sérsic fits does not suggest that the default De Vaucouleurs effective radii from the SDSS catalog are catastrophically wrong for our compact galaxy candidates; if anything, these comparisons suggest that we may in fact be underestimating the sizes of these galaxies by 10–30 %.

### 3.3. A Consistency Check Based on Velocity Dispersions

Assuming that elliptical galaxies are structurally self-similar, the virial theorem implies that  $M_* \propto R_e \sigma^2$ . At fixed mass, galaxies with small sizes should therefore have higher velocity dispersions, with  $\Delta \sigma \propto (\Delta R_e)^{-1/2}$ .

In order to verify that the observed velocity dispersions of our compact galaxy candidates are consistent with their being genuinely small, in the lower panel of Figure 5 we plot the offset from the local size–mass relation for early type galaxies,  $\Delta \log R_e$ , against the offset from the  $M_*$ – $\sigma$  relation,  $\Delta \log \sigma$ ; the  $M_*$ – $\sigma$  relation itself is shown in the upper panel of the Figure. For the lower panel of this plot, we have shifted the Shen et al. (2003) relation upwards in size by 0.05 dex to be consistent with the present data set; our conclusions do not depend on this decision. The greyscale and points show those  $0.066 < z < 0.12$  galaxies with  $^{0.1}(u-r) > 2.5$  and  $M_* > 10^{10.7} M_\odot$ ; the red circles indicate those galaxies that we have identified as compact.

For our compact galaxy candidates, the median offset from the size–mass relation is  $\Delta \log R_e = -0.38$  dex. We would therefore expect a median offset from the  $M_*$ – $\sigma$  relation of  $\Delta \log \sigma = -0.5 \times -0.38 = 0.19$  dex. The median value for  $\Delta \log \sigma$  is 0.12 dex—roughly 85 % of the expected value, and  $\sim 1.5$  times greater than the

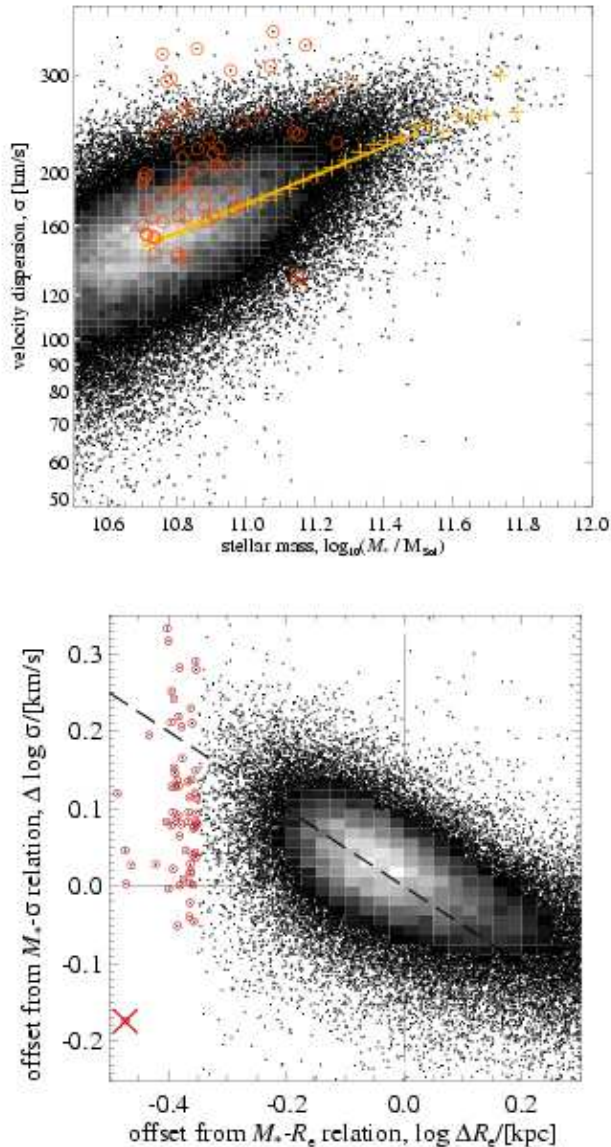


FIG. 5.— Using observed velocity dispersions to validate the measured sizes of our compact galaxy candidates. *Upper panel:* the mass–velocity dispersion relation for red sequence galaxies at  $0.066 < z < 0.12$ . The points and greyscale show the SDSS data. The yellow pluses show the median velocity dispersion in narrow bins of stellar mass; the solid yellow line shows a simple fit to these points for  $10.7 < \log M_* < 11.5$ . The red circles highlight our compact galaxy candidates. *Lower panel:* the offset from the  $M_*$ – $R_e$  relation, plotted against the offset from the  $M_*$ – $\sigma$  relation for  $M_* > 10^{10.7} M_\odot$  galaxies with  $^{0.1}(u-r) > 2.5$ . If the offsets from these two relations is a function of galaxy size, then we expect  $\Delta \log \sigma = -0.5 \times \Delta \log R_e$  (long dashed line). Our compact galaxy candidates are shown as the red circles. In general, the observed velocity dispersions support the idea that our compact galaxy candidates are indeed relatively small; this is particularly true for those with  $\sigma > 200$  km/s. There is one clear exception, marked with a cross in both panels; this galaxy is also the most extreme outlier in Figure 4.

intrinsic scatter in the relation. Overall, these results are fairly consistent, although they do indicate that the sizes may be underestimated and/or the masses may be overestimated at the level of 10–20%. We note that the difference between the default SDSS and the NYU

VAGC size measurements can account for at least half of this effect (see §3.2).

There is one of our compact galaxy candidates however, whose velocity dispersion is clearly inconsistent with its being massive and compact, which we have marked in Figure 5 with a cross; indeed, it has the lowest observed velocity dispersions of all of our compact galaxy candidates. This galaxy is also the biggest outlier in Figure 4. We will discuss this object in more detail in §4.2.

We also note that the observed velocity dispersions of the most extreme outliers from the size–mass relation ( $\Delta \log R_e \lesssim -0.4$ ) are only marginally higher than for galaxies with ‘normal’ sizes. Only one of these candidates ( $\log M_* = 10.73$ ) has  $\Delta \log \sigma > 0.18$  dex; the median value of  $\Delta \log \sigma$  is 0.03 dex. It would seem that the effects of ‘outlier noise’ (*ie.* objects being pushed to the edge of the observed distribution by measurement errors, rather than their true, intrinsic properties) become dominant at these very extreme values of  $\Delta \log R_e$ .

With these caveats, the observed velocity dispersions generally support the idea that the offsets from both the  $M_*$ – $R_e$  and  $M_*$ – $\sigma$  relations for our compact galaxy candidates can be explained by their having small sizes for their masses/velocity dispersions.

#### 4. THE IMPORTANCE OF SELECTION EFFECTS FOR COMPACT GALAXIES

##### 4.1. SDSS Spectroscopic Sample Selection

In order to be targeted for SDSS spectroscopic follow-up (and so to appear in Figure 2), galaxies have to satisfy a complicated set of selection criteria (Strauss et al. 2002). In brief, there is a magnitude cut: objects must be detected at  $> 5\sigma$  significance, and have  $r_p < 17.77$ . Any objects that have been marked as blended and then segmented into smaller objects are rejected, as are any objects that include saturated pixels, or have been deblended from objects with saturated pixels. There are also a series of (low) surface-brightness-dependent criteria that are not relevant here.

The first important selection criterion for our purposes is the star/galaxy separation criteria, since we are concerned about bright, compact galaxies being mistakenly identified as stars. Star/galaxy separation is done on the basis of the difference between the ‘PSF’ and ‘model’ magnitudes in the  $r$  band. (Here, the PSF magnitude is derived by fitting the PSF model to each object, in analogy to the exponential/de Vaucouleurs model fits described in §2.1, and then aperture corrected to  $7''.4$ .) Specifically, objects are only selected for spectroscopic follow-up where:

$$\Delta_{\text{SG}} \equiv r_{\text{PSF}} - r_{\text{model}} \geq 0.3. \quad (2)$$

Further to this star/galaxy discriminator, in order to avoid cross talk between spectroscopic fibers, galaxies with fiber magnitudes  $g < 15$ ,  $r < 15$ , and  $i < 14.5$  are also rejected. Lastly, all objects with  $r_p < 15$  and a Petrosian radius  $\Theta_p < 2''$  are rejected. This criterion was introduced to eliminate “a small number of bright stars that that managed to satisfy equation [2] during the commissioning phase of the survey, when the star/galaxy separation threshold was  $\Delta_{\text{SG}} = 0.15$  mag, and was retained for later runs to avoid saturating the spectroscopic CCDs

(Strauss et al. 2002). Strauss et al. (2002) also note that of the approximately 240000  $r < 17.77$  objects in runs 752 and 756, none were rejected by the  $r_P < 15$ ,  $\Theta_P < 2''$  criterion alone.

In order to model these selections, we need to relate the relevant observed quantities (*viz.*, the apparent Petrosian magnitude,  $r_P$ ,  $gri$  fiber magnitudes, the apparent Petrosian size,  $\Theta_P$ , and the star/galaxy separation parameter,  $\Delta_{SG}$ ) to intrinsic size and stellar mass.

For a given redshift/distance, the intrinsic size can be trivially related to the observed effective radius,  $\Theta_e$ . In order to relate  $r_P$  to  $M_*$ , we have made a simple fit to the relation between stellar mass and absolute magnitude in the observers frame  $r$  band (*ie.* with no K-correction) for red sequence galaxies at  $0.066 < z < 0.12$  with  $M_r > -21$ . Note that this method naturally accounts for mass-dependent trends in, e.g., metallicity along the red sequence. The scatter around this relation is  $\sim 0.06$  dex, with no obvious magnitude dependence. We have derived similar relations for both  $g_P$  and  $i_P$ .

We have also derived empirical relations for  $\Theta_P$ ,  $\Delta_{SG}$ , and the difference between the Petrosian and fiber magnitudes,  $\Delta_{fib} = m_P - m_{fiber}$ , as functions of  $\Theta_e$  and  $r_P$ , using the sample of massive, red sequence galaxies shown in Figure 2. The scatter around these relations is 0.059 dex (15 %), 0.18 mag (18 %), and 0.11 mag (9 %) respectively, with no obvious systematic residuals.

Note that there is a danger of circularity in this argument: any objects that do not satisfy the selection criteria will not be present in the sample that we are using to model the selection criteria. The crucial assumption here, then, is that we can extrapolate the functions for  $\Theta_P(\Theta_e, r_P)$ ,  $\Delta_{SG}(\Theta_e, r_P)$ , and  $\Delta_{fib}(\Theta_e, r_P)$  down past the limits of the spectroscopic sample. In this regard, it is significant both that the derived functions are smooth all the way down to the selection limits, and that we do not see obvious cut-offs in the data associated with these limits.

In Figure 2, we show how these selection criteria translate onto the  $(M_*, R_e)$  plane for several example redshifts between 0.035 and 0.12. The thicker, roughly diagonal, long-dashed lines show the star/galaxy separation criterion; the dotted lines show the ‘cross-talk’ fiber magnitude selection; the thinner, short-dashed boxes show the effect of the ‘saturation’ selection against bright, compact objects. Note that, for example, a galaxy with  $M_* \gtrsim 10^{11} M_\odot$  and  $R_e \lesssim 2$  kpc would not be selected as an SDSS spectroscopic target for  $z \lesssim 0.05$ .

#### 4.2. Compact Galaxies at High and Low Redshifts

In Figure 6 we again show the size–mass relation for our sample of massive, red sequence galaxies at  $0.066 < z < 0.12$ , with the exception that we have not plotted those galaxies rejected as per §3.1. Furthermore, in contrast to Figure 2, we have used the selection limits derived in §4.1 to estimate the relative completeness of the SDSS spectroscopic sample across the  $0.066 < z < 0.12$  volume; these are shown by the contours. These completeness estimates also include the  $r_P < 17.77$  selection limit, which can be seen to affect galaxies with  $M_* \lesssim 10^{10.6} M_\odot$  at the distant end of our redshift window.

For comparison, we have also overplotted the high-redshift samples of D09 (yellow points) and vD08, blue

(blue points). Where we have used size measurements from the  $z$ -band for the SDSS galaxies, these high-redshift studies use the NICMOS F160W filter, which corresponds to rest-frame  $r$  at  $z = 1.6$ , moving close to  $g$  by  $z = 2.3$ . Locally, the difference between  $z$ - and  $r$ -band measured sizes leads to a slightly different slope to the size–mass relation for red sequence galaxies (a slope of 0.65, rather than 0.56). The  $r$ - and  $z$ -band size–mass relations intersect at around  $M_* \sim 10^{10} M_\odot$ ; the mean  $r$ -band size at  $M_* \sim 10^{11} M_\odot$  is 15 % larger than in the  $z$ -band. That is, by using  $z$ -band derived effective radii, we are, if anything, *underestimating* the sizes of the local galaxies in comparison to those at high redshift. Similarly, our decision to use the De Vaucouleurs effective radii given in the basic SDSS catalog, rather than more general Sérsic ones appears to lead to an underestimate of galaxy sizes. In other words, adopting  $r$ - or  $g$ -band derived sizes, or using Sérsic instead of De Vaucouleurs effective radii, would increase the discrepancy between the high- and low-redshift samples.

There is one of our candidates (marked with a cross) that appears to have similar properties to one of the larger of the vD08 galaxies. This turns out to be the galaxy whose observed velocity dispersion is inconsistent with its being genuinely compact (§3.3); where we would predict  $\Delta \log \sigma = 0.24$  dex, or  $\sigma = 310 \pm 70$  km/s, what we observe is  $\Delta \log \sigma = -0.17$  dex and  $\sigma = 129 \pm 14$  km/s. This is also the galaxy with the largest difference between the Sérsic- and De Vaucouleurs-sizes ( $\log R_{Dev}/R_{Ser} = -0.34$ ; see §3.2). Adopting the NYU VAGC Sérsic size measurement is not sufficient to reconcile the observed size and mass with the velocity dispersion: the observed velocity dispersion would still be too small by  $\sim 0.2$  dex. This galaxy also sits nearly 0.25 dex above the median color–mass-to-light relation shown in Figure 1; using the Bell & de Jong (2001) prescription for  $M_*/L$  as a function of  $(B - V)$  leads to a stellar mass estimate that is 0.17 dex lower. Adopting both this mass estimate and the NYU VAGC size estimate, we do find consistency between  $\Delta \log R_e$  and  $\Delta \log \sigma$ . In this sense, this galaxy is the weakest of our compact galaxy candidates—it seems to have had its size underestimated and/or its mass overestimated.

We also stress that the observed velocity dispersions of the candidates that lie furthest from the main size–mass relation suggest that these galaxies have had their sizes significantly underestimated (see §3.3).

If the vD08 galaxies were placed at  $0.066 < z < 0.12$ , the SDSS spectroscopic completeness would typically be  $\gtrsim 75$  %. Note, however, that there are two  $R_e < 0.5$  kpc galaxies from the vD08 sample and one from the D09 sample for which the SDSS completeness is just 20–40 %. The average SDSS completeness for the vD08 galaxies placed at  $0.066 < z < 0.12$  would be 80 %.

If the Kriek et al. (2008a)/vD08 galaxies were not to evolve in either size or number density from  $z \sim 2$  to the present day, we would expect there to be  $\sim 6500$   $M_* > 10^{11} M_\odot$  galaxies with  $\Delta \log R_e < -0.4$  dex at  $0.066 < z < 0.12$ , of which  $\sim 5250$  should appear in the SDSS spectroscopic sample. Instead, we have only one weak candidate.

As an interim conclusion, then, we have shown that

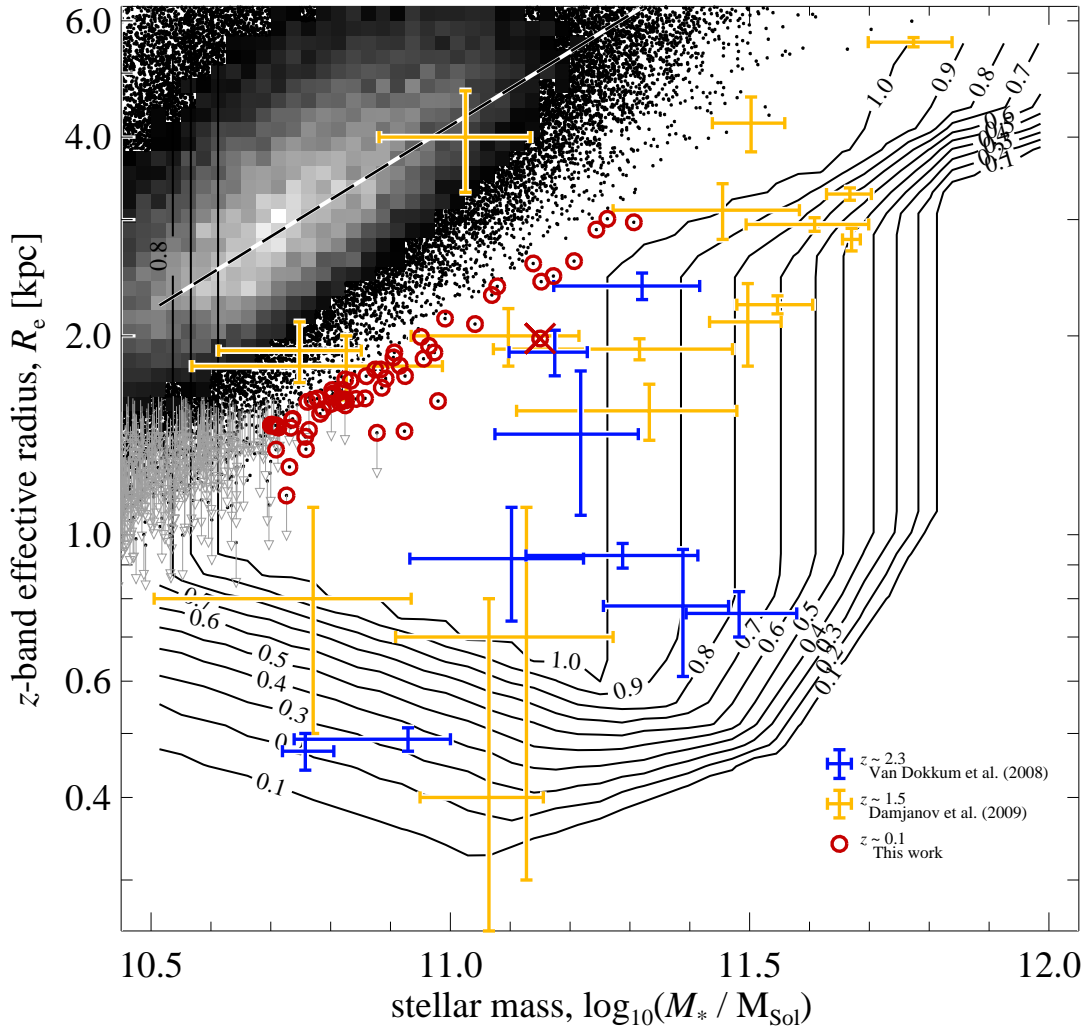


FIG. 6.— The size–mass relation for massive, red sequence galaxies at low and high redshifts. The points and circles are for SDSS galaxies, as in Figure 2; those galaxies that we have rejected as per §3 are not shown. The contours show the relative volume completeness of the SDSS spectroscopic sample for  $0.066 < z < 0.12$ , as marked. The orange points with error bars are the D09 sample of  $1.2 < z < 2.0$  galaxies from the GDDS and MUNICS. The blue points with error bars are the vD08 sample of  $z \sim 2.3$  galaxies from MUSYC. There are no red galaxies in the local universe with sizes and masses comparable to the compact galaxies found at high redshift. This lack cannot be explained by selection effects.

there are no galaxies in the local universe (at least as probed by the SDSS spectroscopic sample) that are directly analogous to the compact galaxies found at high redshift. This dearth of compact galaxies cannot be explained by selection effects. In Appendix A, we confirm this conclusion by searching for compact galaxy candidates from within the SDSS photometric sample, using photometric redshifts.

Moreover, we stress that those galaxies which we have identified as ‘compact’ are not qualitatively similar to the compact galaxies found at higher redshifts, which are offset from the local size–mass relation by at least twice as much again as our local compact galaxy candidates.

#### 4.3. The Number Density of Massive, Compact Galaxies

In Figure 7, we provide a more quantitative statement of our conclusion with respect to the size evolution of

massive galaxies from  $z \sim 2$  to  $z \sim 0.1$  by plotting the size distribution for massive, red galaxies in different mass bins. In this figure, the filled histograms represent the main SDSS spectroscopic sample described above. The horizontal-hatched histograms show, for comparison, the situation at  $z \sim 1.6$ , based on the ten D09 galaxies drawn from the GDDS; similarly, the diagonal-hatched histograms show the nine  $z \sim 2.3$  Kriek et al. (2008a) galaxies with sizes from vD08.

The Kriek et al. (2008a)/vD08 sample is representative, but not complete. In order to derive the densities plotted in Figure 7, we have scaled each of the vD08 galaxies as follows: first, we have normalized the distribution to have a density of  $1.5 \times 10^{-4} \text{ Mpc}^{-3}$ , which corresponds to the total number density of all  $2 < z < 3$  galaxies to the mass limit of Kriek et al. (2008a), derived using the mass function fit given by Marchesini et al. (2008); then, we have scaled this distribution by a fac-

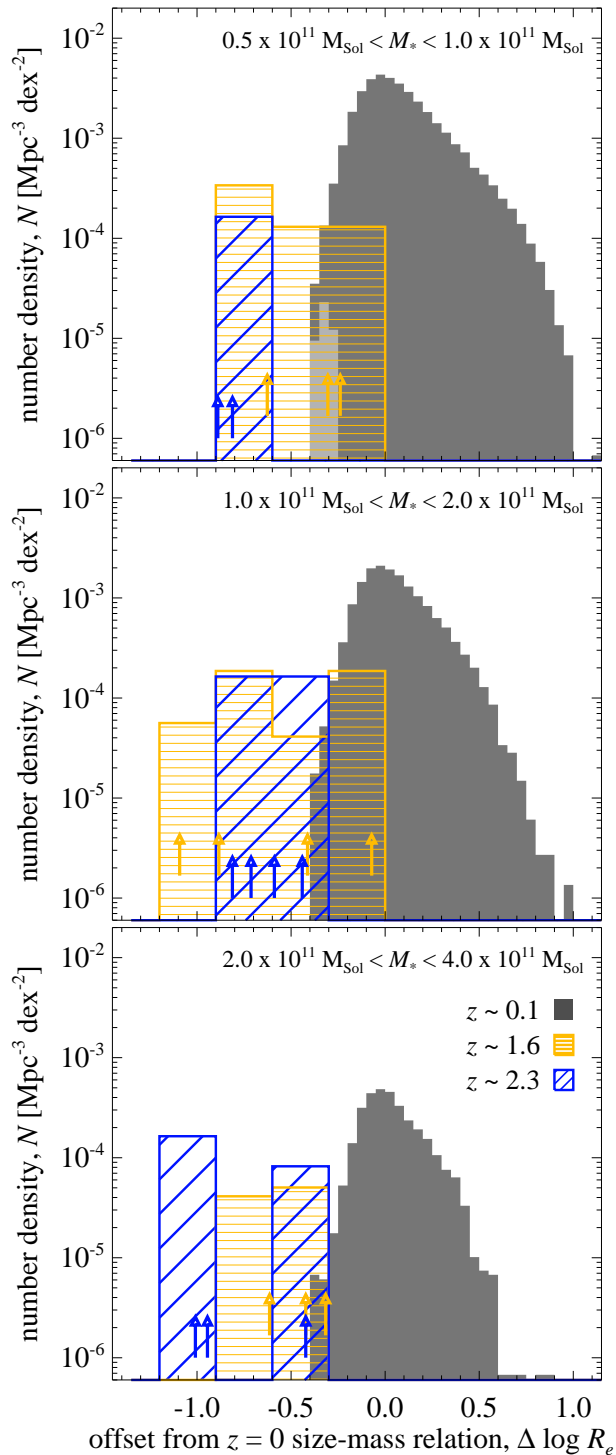


FIG. 7.— The observed size distribution of massive, red galaxies at  $z \sim 0.1$ ,  $z \sim 1.6$ , and  $z \sim 2.3$ ; each panel is for a different mass range as marked. In each panel, the solid histogram represents the SDSS spectroscopic sample. The blue, diagonally-hatched histogram represents the vD08 sample of nine massive, passive galaxies at  $z \sim 2.3$ ; the yellow, horizontally-hatched histogram represents the 10  $z \sim 1.6$  GDDS galaxies from D09. The arrows at the bottom of each panel indicate the positions of the individual high redshift galaxies. The  $z \sim 2.3$  galaxies have to undergo significant structural evolution over  $z \gtrsim 2.3$  to match the properties of local universe galaxies; at least part of this evolution has already occurred by  $z \sim 1.6$ .

tor of 16/36 to count only those galaxies with little or no ongoing star formation from Kriek et al. (2008a) that seem to form a red sequence (Kriek et al. 2008b). For the D09 sample, we are able to use  $1/V_{\max}$  scalings from Glazebrook et al. (2004).

The location of each individual high-redshift galaxy is marked in Figure 7 with an arrow: the slightly lower blue arrows show the vD08 galaxies; the slightly higher yellow arrows are for the D09 galaxies. Clearly, given the small numbers, the uncertainties on these high redshift values are quite large, but they do provide a useful order of magnitude estimate for comparison to the local values.

The clear implication from the comparison between the  $z \sim 0.1$  and  $z \sim 2.3$  data in Figure 7 is that, consistent with the conclusions of vD08, not one of the vD08 galaxies is consistent with the properties of the  $z \sim 0$  galaxy population. With the results we have now presented, we can extend this conclusion by confirming that this discrepancy cannot be explained by selection effects in the low redshift sample.

There are local analogs for less than half of the  $z \sim 1.6$  galaxies, albeit with considerably higher number densities. This would imply that at least some ( $\lesssim 50\%$ ) of the  $z \lesssim 2.3$  evolution has already occurred by  $z \sim 1.6$ .

## 5. DISCUSSION

### 5.1. Compact Galaxy Properties

In Figure 8, we plot the properties of our compact galaxies in comparison to the general massive, red galaxy population. In each panel, the circles highlight our compact galaxies, while the points and greyscale show all galaxies with  $M_* > 10^{10.7} M_{\odot}$ ,  $^{0.1}(u-r) > 2.5$ , and  $0.066 < z < 0.12$ . The large grey boxes with error bars show the mean and standard deviation of each plotted property in quintiles of the velocity dispersion distribution. Similarly, the red boxes with error bars show the mean and standard deviations for our compact galaxy candidates in two bins, separated at  $\sigma = 200$  km/s; the median for this sample.

In each of the panels of Figure 8 (from left to right), we show the equivalent width of the  $H\delta$  line (where negative values imply emission), the luminosity weighted mean stellar metallicity, and the luminosity weighted mean stellar age, as derived from the DR4 SDSS spectra by Gallazzi et al. (2005). Because these estimates are available only for DR4, only around half of our compact candidates can be plotted in these panels, and only 3/10 of those with  $M_* > 10^{11} M_{\odot}$ .

We have also matched our compact galaxy sample to the AGN sample described by Kauffmann et al. (2003b), for SDSS DR4. These AGN hosts have been selected by their  $[\text{OIII}]/\text{H}\beta$  and  $[\text{NII}]/\text{H}\alpha$  emission line ratios; *ie.* the Baldwin, Phillips & Terlevich (1981, BPT) diagram. 34 of our 63 galaxies appear in the DR4 catalog; of these, 11 are classified as AGN on the basis of their emission line ratios. This is slightly higher than the AGN fraction of the parent sample, which is in the range 20–26% for the mass range we are considering. Of the 11 galaxies identified as AGN hosts, five sit on or slightly above the main  $M_* - L_{[\text{OIII}]}$  relation, with  $L_{[\text{OIII}]} \approx 10^6 L_{\odot}$ , four have  $L_{[\text{OIII}]} \sim 10^{7-8} L_{\odot}$ , and one is quite high luminosity, with  $L_{[\text{OIII}]} = 10^{8.7} L_{\odot}$ . These 11 galaxies are marked in

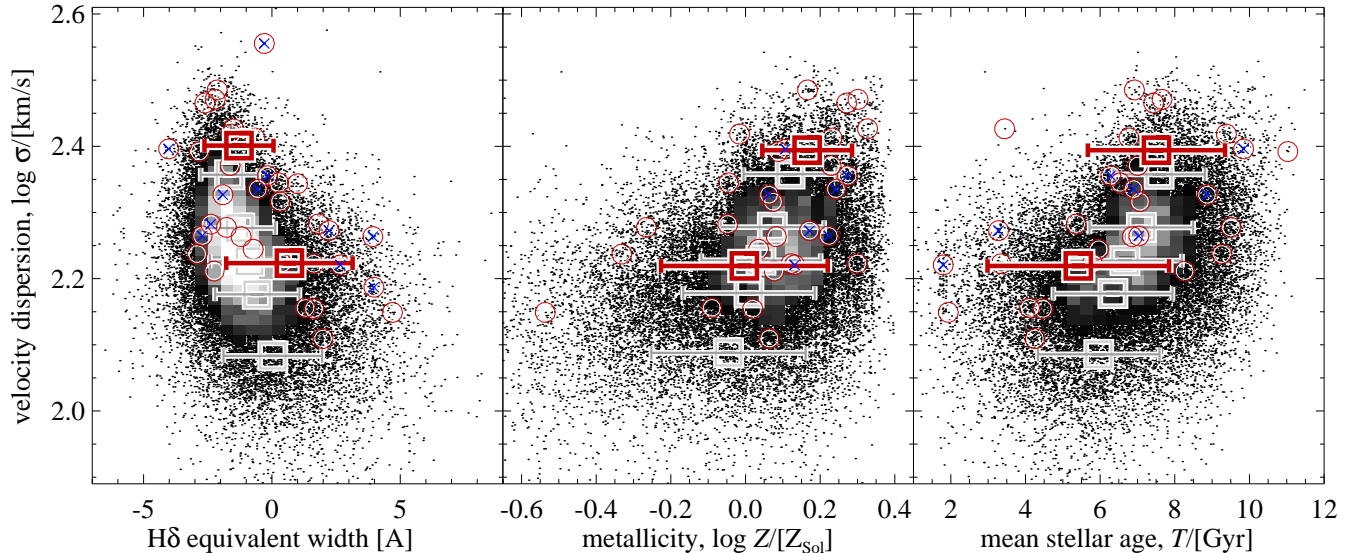


FIG. 8.— The properties of our compact galaxy candidates in comparison to the general population of massive, red sequence galaxies. As in other Figures, the black points and greyscale show the data density of all galaxies with  $M_* > 10^{10.7} M_\odot$ ,  $^{0.1}(u-r) > 2.5$ , and  $0.066 < z < 0.12$ ; the red circles show our compact galaxy candidates. The grey boxes with error bars show the mean and rms scatter in each quantity for quintiles of the velocity dispersion distribution; the red boxes show the same for those of our compact galaxy candidates with  $\sigma < 200$  km/s and  $\sigma > 200$  km/s separately. At fixed velocity dispersion, our compact galaxies have slightly lower than average mean ages and slightly higher metallicities—however, this result is only significant at the  $2\sigma$  level.

each panel of Figure 8 with a small blue cross.

Kauffmann et al. (2003b) also provide revised stellar mass and velocity dispersion measurements for these galaxies. Accounting for the presence of an AGN does not have a major impact on these measurements: the masses and velocity dispersions change at the level of 0.05 dex and 16 km/s, respectively. That is, while it is possible that an optically bright point source may bias the measured sizes of these galaxies downwards, within the stated errors, the AGN does not significantly affect the derived values of  $M_*$  or  $\sigma$ . (It is relevant here that only one of our compact galaxy candidates shows a significant residual point-source after subtracting off the best-fit Sérsic profile, as produced by GALFIT; see §3.2.)

Looking now at Figure 8, it is clear that the majority of our compact galaxy candidates have quite old stellar populations. For the  $\sigma < 200$  km/s bin, the median age is 6 Gyr, although the ages do range from 2 to 10 Gyr, while all but one of the  $\sigma > 200$  km/s candidates have  $T > 6$  Gyr. Among the lower velocity dispersion candidates, there is a clear tendency towards relatively high equivalent widths for H $\delta$  absorption, suggestive of a relatively recent ( $\lesssim 2$  Gyr) star formation event.

At fixed velocity dispersion, our compact galaxy candidates may have slightly higher metallicities, and be slightly younger than average. Using bootstrap-resampling on similar sized samples drawn randomly from the mass-limited sample, and controlling for velocity dispersion, these results are weakly significant at best:  $1.9\sigma$  for the age, and  $< 1\sigma$  for metallicity. Considering only the higher velocity dispersion candidates ( $\sigma > 200$  km/s), the significance of these differences become  $1.9\sigma$  and  $2.2\sigma$  for the age and metallicity offsets, respectively. This weakly significant result should be contrasted with the results of Shankar & Bernardi (2009) and van der Wel et al. (2009), who find that, on average and at fixed dynamical mass, early type galaxies

with higher velocity dispersions (or, equivalently, smaller sizes) have older mean stellar ages.

While the younger mean stellar ages and lower metallicities of our compact galaxy sample are only weakly significant, both would imply a relatively late start to star formation for these galaxies and/or their progenitors. But if these galaxies grow in size through mergers (for example) then it is possible that these galaxies are small not because their formation is delayed relative to other galaxies of the same mass or velocity dispersion, but rather because they have had fewer mergers overall, or perhaps just fewer recent mergers. That is, it may be that, at fixed mass, these compact galaxies are in fact *older*, in the sense that they have been assembled earlier, and existed in (more or less) their present form for longer than other galaxies of the same mass or velocity dispersion.

## 5.2. Comparison to Other Recent Works

In a similar study to this, using sizes and photometry from the NYU VAGC for SDSS DR6, Trujillo et al. (2009) have recently reported the detection of 29  $z < 0.2$  galaxies with  $M_* > 8 \times 10^{10} M_\odot$  and  $R_e < 1.5$  kpc. In contrast, we find just one galaxy from our  $0.066 < z < 0.12$  red sequence galaxy sample that satisfy these mass and size criteria; this implies a difference in volume densities of a factor of 5.5. Most of this difference is explained by the fact that we have preselected our compact galaxies to be red. Of the Trujillo et al. (2009) galaxies, only around 30% (9/29) satisfy our  $^{0.1}(u-r) > 2.5$  criterion, bringing our number densities into agreement. On the other hand, if we also look at  $^{0.1}(u-r) < 2.5$  galaxies, inspected as per §3.1, we find only 7 additional candidates, only 3 of which have  $M_* > 8 \times 10^{10} M_\odot$ ; the most massive of these blue compact galaxy candidates is  $7.2 \times 10^{10} M_\odot$ .

We also note that the Trujillo et al. (2009) galaxies

have considerably smaller observed sizes than the galaxies we consider here. (Recall that we adopt a minimum observed size of  $0''.75$ ; for galaxies with inferred sizes smaller than this, we adopt a size of  $0''.75$  as an upper limit on the true size.) The largest observed size among the Trujillo et al. (2009) sample is  $0''.70$ ; the median is just  $0''.48$ . Enforcing our minimum allowed size of  $0''.75$ , only one of the Trujillo et al. (2009) galaxies, irrespective of color, would have  $R_e < 1.5$  kpc; the median size for the sample would become 2.1 kpc. It is also relevant here that only one of the Trujillo et al. (2009) galaxies is at  $z < 0.12$ ; the other 28 are all found at  $0.12 < z < 0.20$ . This suggests that the Trujillo et al. (2009) size measurements may be biased by inadequate resolution.

The key difference between our compact galaxy sample and that of Trujillo et al. (2009) is that they find a median velocity dispersion which is only 0.04 dex higher than their control sample, even though the mean size and mass are offset from the Shen et al. (2003) relation by  $-0.5$  dex. This discrepancy can only be explained by either very large structural differences, or if the Trujillo et al. (2009) sample is disproportionately affected by large measurement errors in size and/or mass. In this context it is significant that, the observed velocity dispersions for our candidates with  $\Delta \log R_e < -0.4$  dex imply that their very small inferred sizes are produced by large errors in the measured sizes (see §3.3). Only with followup observations will we be able to determine the true nature of the Trujillo et al. (2009) galaxies. In any case, Trujillo et al. (2009) also do not find any galaxies directly comparable to those found at  $z \gtrsim 2$ .

Even more recently, Valentinuzzi et al. (2009) have described a sample of 147 compact galaxies selected from the WIdE-field Nearby Galaxy-cluster Survey (WINGS) of X-ray selected clusters at  $0.04 < z < 0.07$ . Unlike in this work, Valentinuzzi et al. (2009) do find galaxies with properties comparable to the 3 largest vD08 galaxies; similarly, there are local WINGS analogs for 8 of the 10 GDDS galaxies from D09. However, this relies on their scaling the high redshift galaxies' masses down by 0.15 dex to account for the poor treatment of NIR-luminous thermally pulsating asymptotic giant branch (TPAGB) stars in the Bruzual & Charlot (2003) stellar population models. While both Kriek et al. (2009) and Muzzin et al. (2009) show that the stellar masses for the  $z \sim 2.3$  implied by different models vary by  $\sim 0.1$  dex, we have not applied such a correction here.

We note, however, that the high- and low-redshift samples have been treated consistently here, including the fact that all masses were derived from the rest-frame optical. Further, we note that van der Wel et al. (2006) have shown that stellar masses derived from the rest-frame optical and using Bruzual & Charlot (2003) models are consistent with the dynamical masses of  $z < 1$  galaxies, and are unaffected by the TPAGB uncertainties.

The Valentinuzzi et al. (2009) compact galaxies sample is selected by effective surface mass density,  $\Sigma_e = M_*/2\pi R_e^2 > 4 \times 10^9 M_\odot \text{ kpc}^{-2}$ , in the range  $3\text{--}50 \times 10^{10} M_\odot$ . Our compact galaxy selection is roughly equivalent to  $\Sigma_e \gtrsim 3.6 \times 10^9 M_\odot \text{ kpc}^{-2}$ ; nearly half (28/63) of our compact galaxy candidates satisfy the Valentinuzzi et al. (2009)  $\Sigma_e$  criterion. For their sample, Valentinuzzi et al.

(2009) derive a number density of  $1.6 \times 10^{-5} \text{ Mpc}^{-3}$ ; to our mass limit of  $M_* > 10^{10.7} M_\odot$ , this value becomes  $1.2 \times 10^{-5} \text{ Mpc}^{-3}$ . These values are solid lower limits, as they assume that no such galaxies exist outside of the clusters observed by WINGS. For our sample, however, the number density of  $M_* > 10^{10.7} M_\odot$  galaxies with  $\Sigma_e > 4 \times 10^9 M_\odot \text{ kpc}^{-2}$  is just  $2.85 \times 10^{-7} \text{ Mpc}^{-3}$ .

That is, after correcting as best we can for the differential stellar mass limits, our number densities are inconsistent by a factor of more than 40 with those found by Valentinuzzi et al. (2009). Again, our use of  $z$ -band effective radii leads to smaller measured sizes than for bluer bands; this discrepancy would only increase using  $r$ - or  $g$ -band measured sizes. Either our results are badly affected by unexplained selection effects, or there are large discrepancies between our size and mass estimates and those of Valentinuzzi et al. (2009).

We have considered possible spectroscopic selection effects that could bias against bright, compact objects in §4.1, and shown these to be relevant for  $z \lesssim 0.05$ . These effects may well explain why Valentinuzzi et al. (2009) were able to match only a small fraction of their compact galaxies (which have  $0.04 < z < 0.07$ ) to objects in the (DR4) SDSS spectroscopic catalog. We have shown, however, that our  $0.065 < z < 0.12$  results are not strongly affected by these kinds of selection effects (Figure 6, see also Appendix A). Our estimated completeness is more than 60 % for all galaxies in the Valentinuzzi et al. (2009) sample and greater than 90 % for 90 % of the sample. The selection effects considered in §4.1 thus cannot explain the difference in our inferred number densities.

An alternative explanation is that the Valentinuzzi et al. (2009) galaxies only exist in rich clusters, and that SDSS suffers much higher spectroscopic incompleteness in such dense fields because of fiber collisions. A completely independent estimate can be obtained from the Faber et al. (1989) sample: we find that 5/319 of these galaxies have sizes smaller than the mass–size relation by a factor of 2 or more. This fraction for clusters that is approximately 15 times higher than what we find for all galaxies in SDSS. While not conclusive, this does suggest that SDSS may suffer from additional incompleteness beyond the effects we consider here. That said, we note that several studies (e.g. Kauffmann et al. 2004; Park et al. 2007; Weinmann et al. 2009) have found little or no evidence for an environmental dependence of the size–mass relation within SDSS.

Thus we can find no easy explanation for the difference between the Valentinuzzi et al. (2009) results and our own. Here again, velocity dispersion measurements would provide an useful consistency check on the Valentinuzzi et al. (2009) size and mass measurements.

Even despite these differences, however, we note that Valentinuzzi et al. (2009) conclude that—barring large systematic errors in the high-redshift measurements—at least 65 % (*cf.* our value of 100%) of the  $z \sim 2.3$  galaxies from vD08 and at least 20 % (*cf.* our value of 60 %) of the  $z \sim 1.6$  galaxies from D09 have disappeared from the local universe. Accepting the high-redshift results, these galaxies simply cannot evolve passively and statically into the red sequence and/or early type galaxies

found in the local universe.

## 6. SUMMARY AND CONCLUSIONS

The central question of this work has been the existence or otherwise of massive, compact, quiescent and/or early type galaxies in the local universe, and particularly the importance of selection effects in the SDSS spectroscopic sample for such galaxies. We have shown that, especially for lower redshifts ( $z \lesssim 0.05$ ), galaxies with the masses and sizes of those found at  $z \gtrsim 2$  would not be targeted for spectroscopic followup (Figure 2). The main reason for this is not the star/galaxy separation criterion, but rather the exclusion of bright and compact targets in order to avoid saturation and cross-talk in the spectrograph (see §4.1).

We have therefore conducted a search for massive, compact galaxies at  $0.066 < z < 0.12$ , where these selection effects should be less important. We estimate that for  $0.066 < z < 0.12$ , the average completeness for galaxies like those from vD08 and D09 would be  $\gtrsim 25\%$  at worst, and  $\sim 80\%$  on average (Figure 6).

Starting from a sample of massive ( $M_* > 10^{10.7} M_\odot$ ) red sequence ( $^{0.1}(u-r) > 2.5$ ) galaxies, we have selected the 280 galaxies with inferred sizes that are a factor of 2 or more smaller than would be expected from the Shen et al. (2003)  $M_*-R_e$  relation for early type galaxies. In order to confirm their photometry and size measurements, we have visually inspected all of these objects. Unsurprisingly, by selecting the most extreme outliers, a large fraction of these objects ( $\sim 70\%$ ) appear to be instances where the size and/or stellar mass estimates are unreliable (§3.1).

For the 63 galaxies with no obvious reason to suspect their size or stellar mass estimates, there is good agreement between the default SDSS size measurement (based on the 2D light distribution, using a sector-fitting algorithm, and assuming a de Vaucouleurs profile), and those given in the NYU VAGC (based on the azimuthally average growth curve, assuming a more general Sérsic profile). However, particularly for galaxies with high  $n$ , the de Vaucouleurs size measurement is systematically smaller than the Sérsic one, at the level of  $\lesssim 25\%$  (§3.2).

In general, and as expected, our 63 compact galaxy candidates have significantly higher than average velocity dispersions (Figure 5). While it remains possible that the sizes of at least some of our compact galaxy candidates may have had their sizes underestimated by  $\sim 30\%$ , in general, the relatively high observed velocity dispersions support the notion that they are indeed unusually compact given their stellar masses (§3.3).

Among our compact galaxy candidates, there are no galaxies with sizes comparable to those found  $z \sim 2.3$  by vD08; we find analogs for  $\lesssim 50\%$  of the D09 galaxies at  $z \sim 1.6$  (Figures 6 and 7). This lack cannot be explained by selection effects. To confirm this, we have also compared the size–mass diagram, constructed using photometric redshifts, based on both the full photometric sample and the spectroscopic sub-sample (Appendix A). While it is conceivable that SDSS is missing a few

massive, compact galaxies, there are again no signs of galaxies comparable to those of vD08 or D09.

It is not impossible that some systematic errors in the estimation of  $M_*/L_s$  for the high redshift galaxies (e.g., an evolving stellar IMF) mean that their stellar masses are vastly overestimated, however it would require an overestimate of  $\gtrsim 0.7$  dex to reconcile the vD08 galaxies with the sizes of the smallest galaxies we have identified in the SDSS catalog.

Accepting the high redshift observations at face value, then, our results confirm that massive galaxies, both individually and as a population, must undergo considerable structural evolution over the interval  $z \lesssim 2.3$  in order to develop into the kinds of galaxies seen locally—even after star formation in these galaxies has effectively ended. We see some hints that a significant amount of this evolution ( $\lesssim 50\%$ ) may have already occurred by  $z \sim 1.6$ .

The fact that each and every one of the vD08 galaxies must undergo significant structural evolution to match the properties of present-day galaxies implies that the mechanism that drives this growth must apply more or less evenly to all galaxies. To see this, let us assume that some external process drives the size evolution of these galaxies, and that even a single event is sufficient to move an individual galaxy onto the main size–mass relation. Then, we can assume some simple probability distribution for the number of events,  $N$ , among individual galaxies. (For example, we could assume that events occur randomly across the time interval  $z < 2.3$ , or that each galaxy experiences  $N \pm \sqrt{N}$  events.) Now, our results suggest that the number density of vD08-like galaxies drops by at least a factor of 5000 since  $z \sim 2.3$ . In order to ensure that at most 1/5000 galaxies have  $N = 0$  after  $z \sim 2.3$ , simple probabilistic arguments imply that the average galaxy must undergo  $\gtrsim 20$  events. This would imply that a strongly stochastic process like major mergers cannot be the primary mechanism for the strong size evolution of massive galaxies.

Apart from their small sizes and high velocity dispersions, our compact galaxy candidates are not obviously distinct from the general population (Figure 8). If anything, at fixed velocity dispersion, our compact galaxies have stellar populations that are slightly younger than average (at  $\sim 1.9\sigma$  significance). Even so, the majority of these galaxies’ stellar populations are definitely ‘old’, with luminosity-weighted mean stellar ages typically in the range 6–10 Gyr. But if some external mechanism drives the size evolution of these galaxies, we speculate that their small sizes may indicate that they have assumed their present form comparatively *early*, and in this sense they may actually be relatively *old* (see also, e.g., van der Wel et al. 2009). If so, with better understanding of the processes that determine the sizes of early type galaxies, and in particular the role of merging, the properties of these galaxies could provide a means of constraining the evolution of massive galaxies after they have completed their star formation, including their late-time merger histories.

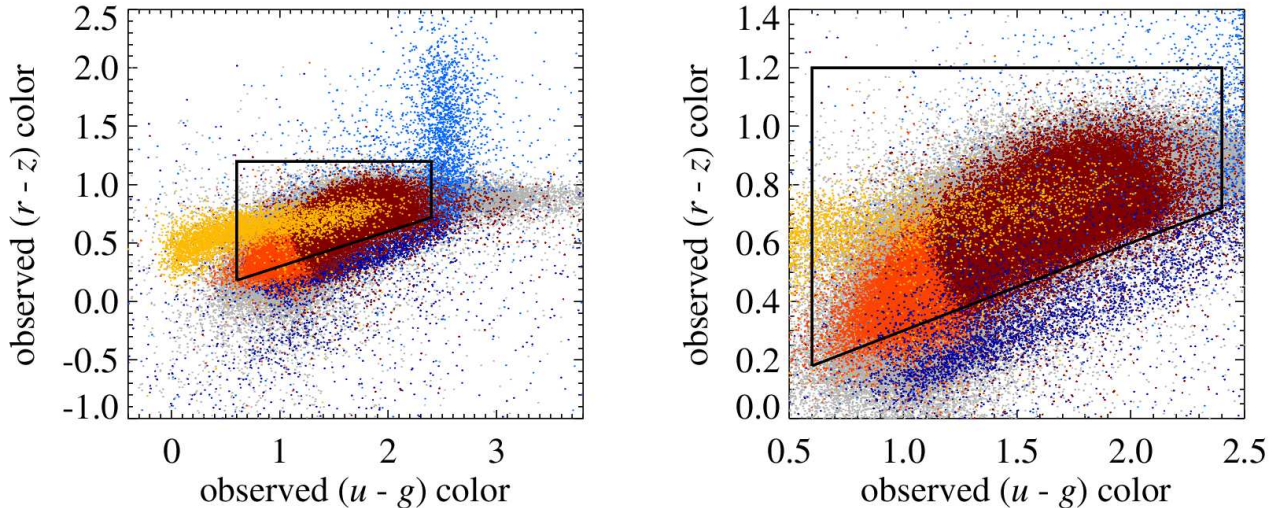


FIG. 9.— Selecting  $z \lesssim 0.1$  galaxies based on color alone. Each panel shows the observed  $(u-g)$ – $(r-z)$  color–color plot for objects in the SDSS spectroscopic sample; the right panel simply shows the central region in greater detail. Points are color-coded according to their spectral classification, *viz.*: galaxies (grey), galaxies with  $0.066 < z < 0.10$  (light red), galaxies with  $0.066 < z < 0.10$  and  $^{0.1}(u-r) > 2.5$  (dark red), quasars (yellow), late-type stars (light blue), and ordinary stars (dark blue). The box shows the color selection that we use to select  $z \lesssim 0.1$  galaxies. This selection should produce a reasonably complete sample of  $z \lesssim 0.1$  galaxies, with some contamination from both stars and quasars. In particular, later-type stars and some quasars have observed SEDs that are very similar to red sequence galaxies at  $z \sim 0.1$ .

## APPENDIX

### A. LOOKING FOR MASSIVE COMPACT GALAXIES IN THE SDSS PHOTOMETRIC SAMPLE

In this Appendix, we present a complementary analysis in which we directly compare the spectroscopic and photometric samples, in order to test the conclusion that the lack of massive, compact galaxies in the spectroscopic sample cannot be explained by the selection effects.

#### A.1. Selecting Galaxies by Color Alone

Before we can address the question of massive compact galaxies in the SDSS photometric sample, we must first devise a means of separating stars and galaxies without selecting on the basis of observed size or light profile. Our method for doing so is shown in Figure 9, which plots the observed (extinction-corrected)  $ugrz$  colors of different classes of objects from the spectroscopic sample; we show: all galaxies (grey),  $0.066 < z < 0.12$  galaxies (bright red), and those with  $^{0.1}(u-r) > 2.5$  (dark red), O–K stars (dark blue), M-type or later stars (light blue), and quasars (yellow).

The black box shown in Figure 9 shows our criteria for selecting  $0.066 < z < 0.12$  galaxies based on their  $ugrz$  colors:

$$\begin{aligned} 0.6 < (u-g) < 2.4 \quad \text{and} \\ 0.3 \times (u-g) < (r-z) < 1.2 . \end{aligned} \quad (\text{A1})$$

Again, we apply this selection in terms of model colors. Note how, whereas the stellar sequence is reasonably well separated from the region of color space occupied by galaxies for  $(u-g) \lesssim 2.5$ , beyond this point, the late-type stellar sequence turns up, such that late-type stars and galaxies are blended. In the most general terms possible, the mean galaxy redshift increases towards redder  $(u-g)$  colors. This means that our ability to distinguish red galaxies from late-type stars on the basis of their optical SEDs is limited to  $z \lesssim 0.12$ .

In the right-hand panel of Figure 9, we zoom in on this selection region. From this panel, it is clear that a large proportion of quasars will also be included in our color-selected ‘galaxy’ sample. Similarly, it is clear that this color selection is not 100 % efficient in excluding stars from our sample: more quantitatively, with this selection we are able to exclude more than 80 % of spectroscopically identified stars that are given  $0.066 < z_{\text{phot}} < 0.12$ , while retaining more than 97 % of all  $0.066 < z_{\text{phot}} < 0.12$  galaxies. Furthermore, it should be remembered that stars are already heavily selected against for the spectroscopic sample plotted in Figure 9; the relative number of stellar ‘contaminants’ may well be considerably higher for the photometric sample.

#### A.2. Photometric Redshifts and Stellar Mass Estimates

A major improvement in DR7 is a complete revision in how the basic (photoz) photometric redshifts are derived (Abazajian et al. 2009). Rather than using some combination of synthetic template spectra to reproduce the observed

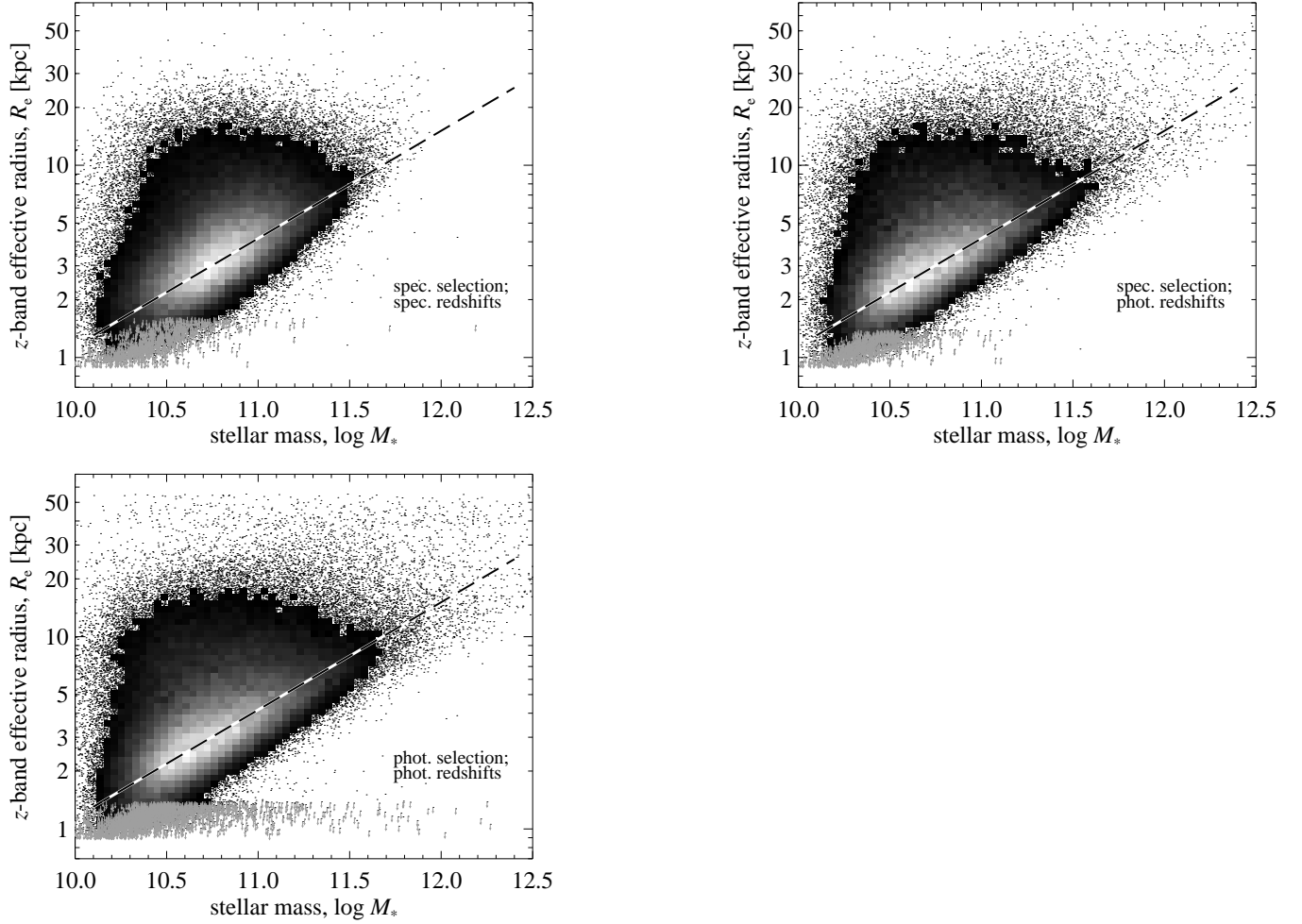


FIG. 10.— The size–mass plot for massive, red sequence galaxies at  $0.066 < z < 0.12$ , based on the spectroscopic and the full photometric SDSS catalogs. Each panel shows the sizes and masses of galaxies based on, from top to bottom, the spectroscopic sample using spectroscopic redshifts, the spectroscopic sample using photometric redshifts, and the photometric sample using photometric redshifts; in each case, only those objects inferred to have  $^{0.1}(u-r) > 2.5$ , and  $0.066 < z < 0.10$  are shown. In panel 3, many more objects with inferred sizes  $\lesssim 0.3$  kpc can be seen; these are largely stars misclassified (in terms of their photometric redshifts) as galaxies. For  $M_* \lesssim 10^{10.8} M_\odot$  and  $R_e \lesssim 10^{-0.2}$  kpc, comparison between panels 2 and 3 suggest that there may be a few additional galaxies in the photometric sample that do not appear in the spectroscopic sample.

colors of individual galaxies, the new `photoz` algorithm directly compares the observed photometry of individual galaxies to that of galaxies that have spectroscopic redshifts. Specifically, for each individual object, the algorithm finds the 100 closest neighbours in *ugriz* color space, and fits a hyper-plane to these points, rejecting outliers; the redshift is then determined by interpolating along this 4D surface. In comparison to the DR6 algorithm, this reduces the RMS redshift error by more than 75 % ( $\langle \Delta z \rangle = 0.025$ ), and significantly reduces systematic errors (Abazajian et al. 2009).

For this analysis, rather than full SED-fit stellar mass estimates assuming the photometric redshifts, we will simply make use of the empirical relation between  $^{0.1}(g-i)$  color and  $M_*/L$  (Equation 1). In this way, we are able to recover the  $z_{\text{spec}}$ -derived, SED-fit  $M_*/L$ s of the sample of galaxies shown in Figure 1 to 0.045 dex ( $1\sigma$ ); including the effects of photometric redshift errors, k-corrections, and  $M_*/L$  errors, the total ( $1\sigma$ ) error in  $M_*$  is 0.13 dex. This should be compared to the median formal error on the original SED-fit stellar mass estimates, 0.10 dex; that is, the errors on  $M_*$  based on photometric masses (adding these two errors in quadrature) are only about 60 % greater than those based on spectroscopic redshifts.

### A.3. The Size Distribution of Massive, Red Sequence Galaxies

In Figure 10, we show three size–mass diagrams corresponding to, from top to bottom: (a.) the spectroscopic sample, analyzed using spectroscopic redshifts; (b.) the spectroscopic sample, analyzed using photometric redshifts; and (c.) the photometric sample, analyzed using photometric redshifts. In all three cases, the only selections applied to each sample are on photometric type (to exclude optical artifacts, etc., we require either a star or galaxy type classification) and *ugrz* color (to exclude stars); then, as in Figures 2 and 6, we are only showing those galaxies inferred to have  $0.066 < z < 0.12$  and  $^{0.1}(u-r) > 2.5$ . Again, objects with measured sizes smaller than 0.75 are shown as upper

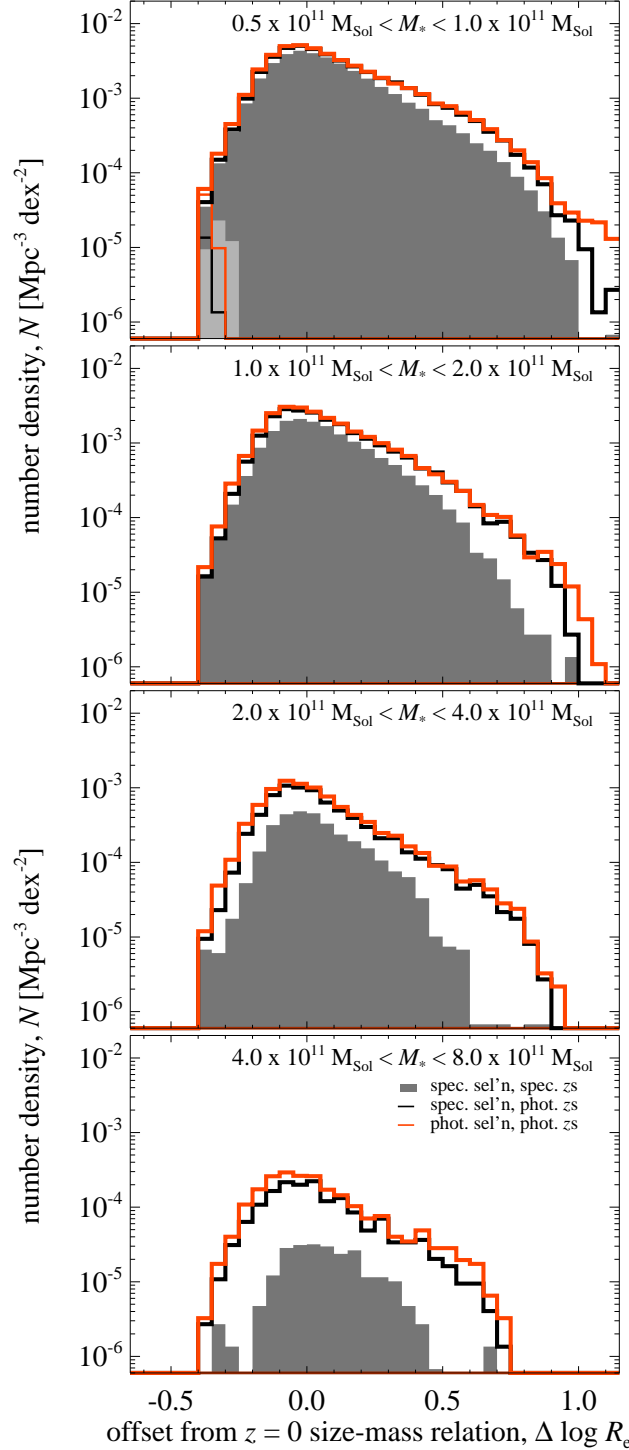


FIG. 11.— The observed size distribution of massive, red galaxies at  $0.066 < z < 0.12$ ; each panel is for a different mass range as marked. In each panel, the solid histogram represents the SDSS spectroscopic sample, analyzed using spectroscopic redshifts. The black and red histograms are the SDSS spectroscopic and photometric samples, respectively, analyzed using photometric redshifts. We have visually inspected all objects with inferred  $M_* > 10^{11} M_\odot$  and  $\Delta R_e < -0.5$  dex; not one of these objects is a plausible massive, compact galaxy candidate. The fact that the shape of the red histogram does not differ significantly from that of the black histogram for  $\Delta R_e > -0.5$  dex indicates that the spectroscopic sample is not significantly biased against compact galaxies.

limits, assuming a size of  $0''.75$ . When comparing these three different analyses, the difference between (a.) and (b.) shows the effect of using spectroscopic versus photometric redshifts, and the difference between (b.) and (c.) shows the difference between the SDSS spectroscopic and photometric selection. That is, the comparison between (b.) and (c.) gives a direct indication of the level of incompleteness in the spectroscopic sample.

Looking at panels (a.) and (b.), it is clear that the use of photometric redshifts produces a considerably greater

scatter in the size–mass diagram, including a rather large number of galaxies with inferred stellar masses of  $10^{12} M_{\odot}$  or greater. There is a clear excess of unresolved objects with inferred stellar masses greater than  $\sim 10^{11} M_{\odot}$  in panel (b.) in comparison to panel (a.) However, we already know from section 3 that there are no objects in the spectroscopic sample with these sizes and masses—these objects cannot be genuine compact galaxies. Of the 34 with inferred  $M_* > 10^{11} M_{\odot}$ , 16 of these objects are spectrally identified as being stars, and one as a quasar at  $z = 0.102$ . Of the 17 spectrally confirmed galaxies, all have  $|z_{\text{phot}} - z_{\text{spec}}| \gtrsim 0.02$ . Of these, 15 have had their redshifts, and thus stellar masses, seriously overestimated; the other two are at  $z > 0.12$ , and so have had their intrinsic sizes underestimated.

Turning now to the comparison between panels (b.) and (c.), the first point to make is that the excess of unresolved sources is even more pronounced. We have matched all of these objects to the 2MASS point source catalog in order to investigate their NIR colors. 90 % of these objects fall in the stellar region of the  $(J - K)$ – $K$  color–magnitude plot; similarly, 80 % fall in the stellar region of a  $(g - z)$ – $(J - K)$  color–color plot.

Further, we have visually inspected the 434 objects with inferred  $M_* > 10^{11} M_{\odot}$  and with sizes smaller than the main  $M_*$ – $R_e$  relation by 0.4 dex or more. Roughly 70 % of these objects are obviously stars: 133 come from crowded Galactic fields covered as part of SEGUE; 126 are double stars; 49 have clear diffraction spikes and/or are clearly saturated. Another 12 objects have been cross-matched with the USNO-B star catalog (within  $1''$ ), and have measured proper motions of  $1$ – $4''/\text{yr}$ . 19 objects are the central point sources of very large spiral galaxies; most of these are also found in the ROSAT and/or FIRST catalogs. We also note that there are 17 very small disk or irregular galaxies with red point sources at or very near their centers. Most of these also have proper motion measurements from the USNO-B catalog, and several are spectrally identified as late type stars; it seems plausible that these galaxies simply have foreground stars coincidentally superposed very near their centers.

In short, of the 434 objects from the full photometric sample that, on the basis of photometric redshifts, are inferred to have  $M_* > 10^{11} M_{\odot}$  and  $\Delta R_e < -0.4$  dex, not one remains as a viable compact galaxy candidate.

#### A.4. Estimating the Importance of Spectroscopic Selection Effects

The conclusion from both the analyses that we have now presented is that there are no galaxies in the local universe with sizes and masses comparable to the compact galaxies found at higher redshifts. In Figure 11, we provide a more quantitative statement of this conclusion, by plotting the size distribution for massive, red galaxies in different mass bins.

In this figure, the filled histograms represent the main SDSS spectroscopic sample, analyzed using spectroscopic redshifts, as in §3. The heavy black and red histograms represent the spectroscopic and photometric samples, respectively, analyzed using photometric redshifts, as in §A.3. In all cases, objects excluded on the basis of visual inspection are not included; this accounts for the sharp cutoffs at  $\Delta \log R_e = -0.3$  and at  $\Delta \log R_e = -0.4$  for the filled and open histograms, respectively. Immediately above these cutoffs, where we have not visually inspected individual objects, but where there is likely to still be significant contamination, these distributions should be regarded as upper limits on the true distribution. In the upper panel, we plot those objects with observed sizes smaller than  $0''.75$  separately as the light grey filled histogram, and the thin black and red histograms.

As in §A.3, the difference between the filled and solid black histogram, both of which are derived from the spectroscopic sample, shows the increased scatter due to the use of photometric redshifts.

Similarly, the difference between the black and red histograms show the difference between the spectroscopic and photometric samples, and so allow a quantification of the bias in the spectroscopic sample. By simply tallying the numbers of galaxies with  $-0.4 < \Delta \log R_e < -0.3$ , we find that the ‘completeness’ (the ratio between the number of galaxies in the spectroscopic sample compared to the full photometric sample) is 75 %, 68 %, 67 %, and 43 % for each of these mass bins, from lowest to highest.

In order to improve on these estimates, we have done the following. Using the approach described above, we have assigned each object a weight according to its  $z_{\text{phot}}$ –derived mass and size. Then, going back to the spectroscopic sample, we use these to compute the mean weight in cells of  $z_{\text{spec}}$ –derived mass and size. The completeness contours we derive in this way are in good qualitative agreement with those shown in Figure 2, although they suggest incompleteness at the 2–5 % level for mean–sized galaxies with  $M_* \gtrsim 10^{11} M_{\odot}$ . Using these values to estimate the number of  $M_* > 10^{11} M_{\odot}$  galaxies with  $\Delta R_e < -0.3$  dex, this suggests that the spectroscopic sample is missing on the order of 4 such galaxies.

## REFERENCES

- Abazajian K N, et al., 2009, *ApJSS* (in press, arXiv:08120649v2)
- Baldwin, J.A., Phillips, M.M., Terlevich, R., 1981, *PASP*, 93, 5
- Bell E F, de Jong R S, 2001, *ApJ* 550, 212
- Bell E F, Zheng X Z, Papovich C, Borch A, Wolf C, Meisenheimer K, 2007, *ApJ* 663, 834
- Bezanson R, van Dokkum P G, Tal T, Marchesini D, Kriek M, Franx M, Coppi P, 2009, *ApJ* 697, 1290
- Bell E F, McIntosh D H, Katz N, Weiberg M D, 2003, *ApJSS* 149, 289
- Blanton M R, Schlegel D J, Strauss M A et al., 2005, *AJ* 129, 2562
- Blanton M R & Roweis S, 2007, *ApJ* 133, 734
- Bruzual G & Charlot S, 2003, *MNRAS* 344, 1000
- Buitrago F, Trujillo I, Barro G, Gallego J, Zamorano J, Conselice C J, 2008, *ApJL* 687, 61
- Cappellari M, di Serego Alighieri S, Cimatti A, Daddi E, Renzini A, Kurk J et al., 2009, *ApJ* (submitted; arXiv:0906.3648v1)
- Cattaneo A, Dekel A, Faber S M, Guiderdoni B, 2008, *MNRAS* 389, 567
- Chabrier G, 2003, *ApJ* 586, L133
- Cimatti A, Daddi E, Renzini A, Cassata P, Vanzella E, Pozzetti L, Cristiani S, Fontana A, Rodighiero G, Mingoli M, Zamorani G, 2004, *Nature* 430, 184
- Cimatti A, Cassata P, Pozzetti L, Kurk J, Mignoli M, Renzini A, Daddi E, Bolzonella M, Brusa M, Rodighiero G, Dickinson M, Franceschini A, Zamorani G, Berta S, Rosati P, Halliday C, 2008, *A&A* 482, 21
- Croton D J, Springel V, White S D M, De Lucia G, Frenk C S, Gao L, Jenkins A, Kauffmann G, Navarro J F, Yoshida N, 2006, *MNRAS* 365, 11
- Daddi E, Renzini A, Pirzkal N, Cimatti A, Malhotra S, Stiavelli M, Xu C, Pasquali A, Rhoads J E et al., 2004, *ApJ* 626, 680
- Daddi E, Renzini A, Cimati A, Malhotra S, Stiavelli M, Xu C, Pasquali A, Rhoads J E, Brusa M, di Serego Alighieri S, Ferguson H C, Koekemoer A, Moustakas L A, Panagia N, Windhorst R A, 2005, *ApJ* 626, 680
- Damen M et al., 2009, *ApJ* 690, 937
- Damjanov I, McCarthy P J, Abraham R G, Glazebrook K, Yan H et al., 2009, *ApJ* (accepted; arXiv:0807.1744v3)
- Dekel A, Birnboim Y, 2006, *MNRAS* 368, 2
- De Lucia G, Springel V, White S D M, Croton D, Kauffmann G, 2006, *MNRAS* 366, 2, 499
- Faber S M Wegner G, Burnstein D, Davies R L, Dressler A, Lynden-Bell D, Terlevich R J, 1989, *ApJS* 69, 763
- Faber S M et al., 2007, *ApJ* 665, 265
- Fan L, Lapi A, De Zotti G, Danese L, 2009, *ApJ* 689, L101
- Franx M et al., 2003, *ApJ* 587, L79
- Franx M, van Dokkum P G, Förster-Schreiber N M, Wuyts S, Labbé I, Toft S, 2008, *ApJ* 688, 770
- Gallazzi A, Charlot S, Brinchmann J, White S D M, Tremonti C A, 2005, *MNRAS* 362, 41
- Glazebrook K, Abraham R G, McCarthy P J, Savaglio S, Chen H-W, Crampton D, Murowinski R, Jørgensen I, Roth K, Hook I, Marzke R O, Carlberg R G, 2004, *Nature* 430, 181
- Guo Y, McIntosh D H, Mo H J, Katz N, van den Bosch F C, Weinberg M, Weinmann S M, Pasquali A, Yang X, 2009, *MNRAS* (submitted; arXiv:0901.1150)
- Hopkins P F, Bundy K, Murray N, Quataert E, Lauer T, Ma C-P, 2009, *MNRAS* (submitted, arXiv:0903.2479)
- Juneau S et al., 2005, *ApJ* 619, L135
- Khochfar S & Silk J, 2009, *MNRAS* 397, 506
- Kriek M, van Dokkum P G, Franx M, Quadri R, Gawiser E, Herrera D Illingworth G D, Labbé I, Lira P, Marchesini D, Rix H-W, Rudnick G, Taylor E N, Urry M C, Wuyts S, 2008, *ApJL* 649, 71
- Kriek M, van Dokkum P G, Franx M, Illingworth G D, Marchesini D, Quadri R, Rudnick G, Taylor E N, Förster-Schreiber N M, Gawiser E, Labbé I, Lira P, Wuyts S, 2008, *ApJ* 677, 219
- Kriek M, van der Wel A, van Dokkum P G, Franx M, Illingworth G D, 2008, *ApJ* 682, 896
- Kriek M, van Dokkum P G, Labbé I, Franx M, Illingworth G D, Marchesini D, Quadri R, 2009, *ApJ* 700, 221
- Kauffmann G, Heckman T M, White S D M et al., 2003, *MNRAS* 341, 33
- Kauffmann G, Heckman T M, Tremonti C et al., 2003b, *MNRAS* 346, 1055
- Kauffmann G, White S D M, Heckman T, Ménard B, Brinchmann J, Charlot S, Tremonti C, Brinkmann J, 2004, *MNRAS* 353, 713
- Longhetti M, Saracco P, Severgnini P, Della Caca R, Mannucci F, Bender R, Drory N, Feulner G, Hopp U, 2007, *MNRAS* 374, 614
- Marchesini D, van Dokkum P G, Förster-Schreiber N M, Franx M, Labbé I, Wuyts S, 2008, *ApJ* (submitted; arXiv:0811.1773)
- McCarthy P J, Le Borgne D, Crampton D, Chen H-W, Abraham R G, Glazebrook K, Savaglio S et al., 2004, *ApJ* 614, L9
- McCarthy P J, 2004b, *ARAA*, 42, 477
- Menci N, Fontana A, Giallongo E, Salimbeni S, 2005, *ApJ* 632, 49
- Muzzin A, Marchesini D, van Dokkum P G, Labbé I, Kriek M, Franx M, 2009, *ApJ* (submitted; arXiv 0906.2012)
- Naab T, Johansson P H, Ostriker J P, 2009, *ApJ* 699, L178
- Padmanabhan N, Schlegel D J, Finkbeiner D P et al. 2008, *ApJ* 674, 1217
- Park C, Choi Y-Y, Vogeley M S, Gott J R, Blanton M R, 2007, *ApJ* 658, 898
- Peng C Y, Ho L C, Impey C D, Rix H-W, 2002, *AJ* 124, 266
- Saracco P, Longhetti M, Andreon S, 2009, *MNRAS* 392, 718
- Shankar S & Bernardi M, 2009, *MNRAS* 396, L76
- Shen S, Mo H J, White S D M et al., 2003, *MNRAS* 343, 978
- Stoughton C et al., 2002, *AJ* 123, 485
- Strauss M A, Weinberg S H, Lupton R H, Narayanan V K et al., 2002, *AJ*, 124, 1810
- Taylor E N, Franx M, van Dokkum P G et al., 2009, *ApJS* (in press; arXiv:0903.3051v1)
- Thakar A R, Szalay A, Fekete G, Gray J, 2008, *CSE* 10, 30
- Toft S, van Dokkum P G, Franx M, Labbé I, Förster-Schreiber N M, Wuyts S, Rudnick G, Zirm A, Kriek M, van der Werf P, Blakeslee J P, Illingworth G, Rix H-W, Papovich C, Moorwood A, 2007, *ApJ* 671, 285
- Trujillo I, Förster-Schreiber N M, Rudnick G, Barden M, Franx M, Rix H-W, Caldwell J A R, McIntosh D, Toft S, Häussler B, Zirm A, van Dokkum P G, Labbé I, Moorwood A, Röttgering H, van der Wel A, van der Werf P, van Starckenburg L, 2006, *ApJ* 650, 18
- Trujillo I, Conselice C, Bundy K, Cooper M C, Eisenhardt P, Ellis R C, 2007, *MNRAS* 382, 109
- Trujillo I, Cenarro A J, de Lorenzo-Cáceres A, Vazdekis A, de la Rosa I G, Cava A, *ApJL* 692, L118
- Valentinuzzi T, Fritz J, Poggianti B M, Bettoni D, Cava A, Fasano G, Onofrio M, Couch W J, Dressler A, Moles M, Moretti A, Omizzolo A, Kjaergaard P, Vanzella E, Verela J, 2009, *ApJ* (submitted; arXiv:0907.2392)
- van der Wel A, Franx M, Wuyts S, van Dokkum P G, Huang J, Rix H-W, Illingworth G D, 2006, *ApJ* 652, 97
- van der Wel A, Holden B, Zirm A W, Franx M, Rettura A, Illingworth G D, Ford H C, 2008, *ApJ* 688, 48
- van der Wel A, Bell E F, van den Bosch F C, Gallazzi A, Rix H-W, 2009, *ApJ* 698, 1232
- van Dokkum P G et al., 2006, *ApJ* 638, 59
- van Dokkum P G, Franx M, Kriek M et al., 2008, *ApJL* 677, L5
- van Dokkum P G, Kriek M, Franx M, 2009, *Nature* (accepted; arXiv:0906.2778)
- York D G et al., 2000, *AJ* 120, 2131
- Weinmann S M, Kauffmann G, van den Bosch F C, Pasquali A, McIntosh D H, Mo H, Yang X, Guo Y, 2009, *MNRAS* 394, 1213
- Wuyts S, Labbé I, Franx M, Rudnick G, van Dokkum P G, Fazio G G, Förster-Schreiber N M F, Huang J, Moorwood A F M, Rix H-W, Röttgering H, van der Werf P, 2007, *ApJ* 655, 51
- Zheng X Z, Bell E F, Papovich C, Wolf C, Meisenheimer K, Rix H-W, Rieke G H, Somerville R, 2007, *ApJL* 661, 41
- Zirm A W, van der Wel A, Franx M, Labbé I, Trujillo I, van Dokkum P G, Toft S, Daddi E, Rudnick G, Rix H-W, Röttgering H, van der Werf P, 2007, *ApJ* 656, 66